

# Polymer Adsorption on Curved Surfaces

Handan Arkin<sup>1,2,\*</sup> and Wolfhard Janke<sup>1,†</sup>

<sup>1</sup>*Institut für Theoretische Physik, Universität Leipzig, Postfach 100 920, D-04009 Leipzig, Germany*

<sup>2</sup>*Department of Physics Engineering, Faculty of Engineering,  
Ankara University, Tandogan, 06100 Ankara, Turkey*

The conformational behavior of a coarse-grained finite polymer chain near an attractive spherical surface was investigated by means of multicanonical Monte Carlo computer simulations. In a detailed analysis of canonical equilibrium data over a wide range of sphere radius and temperature, we have constructed entire phase diagrams both for non-grafted and end-grafted polymers. For the identification of the conformational phases, we have calculated several energetic and structural observables such as gyration tensor based shape parameters and their fluctuations by canonical statistical analysis. Despite the simplicity of our model, it qualitatively represents in the considered parameter range real systems that are considered in experiments. The work considered here could have experimental implications from protein-ligand interactions to designing nano smart materials.

## I. INTRODUCTION

The interaction of macromolecules with differently shaped substrates is particularly important for interdisciplinary research and nano-technological applications including, e.g., the fabrication of biosensors [1] and peptide adhesion [2] to metals [3, 4] or semiconductors [5–7]. The knowledge of structure formation for a variety of interfaces has therefore been a challenging subject of numerous experimental, theoretical and computational investigations. This includes thermodynamic studies of polymers at planar surfaces [8–24], and also under pulling force [25, 26], and at curved surfaces such as nano-tubes, nano-strings and nano-particles [27–31]. Polymer adsorption on flat surfaces plays an important role within a wide perspective. Due to the many possible applications, these "hard-soft" hybrid systems have been extensively studied from all aspects. Recently, employing a single-chain mean-field theory for polymers grafted to a flat surface has featured different morphologies for which, by controlling the self-assembly conditions, non-aggregated chains can coexist with micelles [35]. The understanding of the conformational properties of a polymer requires systematic studies because of the cooperative effect of the monomers in response to different system conditions. The structuring effect of an attractive substrate results in a rich phase behavior caused by the competition between monomer-monomer and monomer-surface interaction. By performing Monte Carlo simulations for detailed atomistic and generic coarse-grained lattice and continuum models, many studies have been done to investigate nano-particle-polymer interactions for different geometries, such as cylinder and sphere [32]. Tanaka *et al.* [33] examined the freezing transition of compact polyampholytes, for both single and multiple chains. There has been a number of studies of these systems to determine the effects of surface charge densities [34] and solvent conditions on the morphologies of polymer chains. Using computer simulations, Barr and Panagiotopoulos [36] studied a system of polymers grafted to a spherical nano-particle in salt solution to gain insight into the conformational behavior of polymers on curved surfaces. Silver nano-particles have also been considered experimentally as catalyst for enhanced amyloid peptide fibrillation [37, 38]. Furthermore adsorption of charged chains such as polyelectrolytes by oppositely charged surfaces is also an important aspect in surface and colloidal science [39, 40]. Because of the electrostatic attractional potential between polyelectrolyte chains and surfaces the charged chains tends to be adsorbed onto the surface. These studies are also extended to opposite charge blocks on the chains [41], and Dobrynin, Rubinstein addressed typical adsorption regimes for a salt free environment using scaling law arguments [42, 43]. The interaction between polyelectrolytes and small spheres of opposite charge is of interest for many problems such as interaction between polyelectrolytes and micelles or formation of nucleosomal complex between DNA and proteins [44, 45].

Recently we have investigated the purely steric confinement effect of a spherical cage on a generic coarse-grained flexible polymer chain to determine the influence on the location of the collapse and freezing transitions [46]. Another hybrid system under consideration was a polymer chain inside an attractive spherical cage for which we have constructed the phase diagram depending on the attraction strength of the sphere inner wall and the temperature [47, 48] and investigated the ground-state properties [49]. We have also compared the results with the case of an attractive flat

---

\*E-mail: Handan.Olgar@eng.ankara.edu.tr

†E-mail: Wolfhard.Janke@itp.uni-leipzig.de;

Homepage: <http://www.physik.uni-leipzig.de/CQT.html>

surface [50]. Both systems exhibit a rich phase behavior ranging from highly ordered, compact to extended, random coil structures.

Here, we consider the opposite situation: A nano-sphere whose attractive outer spherical surface is the target for the adsorbing polymer. This problem could have practical implications for a broad variety of applications ranging from protein-ligand binding, designing smart sensors to molecular pattern recognition [51–54] and for the discovery of new drugs that bind to specific receptors. Therefore it is interesting to study the adsorption of macromolecules on different types of substrates and identify the conformational changes that a polymer can experience at the interface. In this paper, we are going to investigate a simple coarse-grained polymer model interacting with a spherical surface of varying curvature by means of multicanonical Monte Carlo computer simulations. This method enables us to give an overview of the different structural phases of a flexible polymer chain over a wide range of sphere radius and temperature. In a comparative study, we consider the two cases of non-grafted and end-grafted polymer chains.

The rest of the paper is organized as follows. In Section II the model system is described in detail. Our model is a simple model that enables changing parameters in a broad scale, which provides mapping different real systems which are taken into account in experiments. We kept the adsorption field constant in this study (whereas we varied the adsorption strength in another earlier study) and varied the radius of the nano-particles and observed qualitatively the described scenarios. Then, in Section III the multicanonical Monte Carlo simulation method is briefly reviewed and the measured observables are introduced. Section IV presents and discusses the main results, the phase diagrams for the two systems under consideration. Finally, Section V concludes the paper with a summary of our findings.

## II. MODEL

### A. Bead-stick polymer model

The polymer chain is described by a generic, coarse-grained continuum model for homopolymers which has also been used for studies of heteropolymers in the frame of the hydrophobic-polar model [55]. As in lattice models, the adjacent monomers are connected by rigid covalent bonds. Thus, the distance is kept fixed and set to unity. The contact interaction of lattice models is replaced by a distance-dependent Lennard-Jones (LJ) potential accounting for short-range excluded volume repulsion and long-range interaction. An additional interaction accounts for a bending energy (very weak in our case) of any pair of successive bonds.

The LJ potential of nonbonded monomers is of standard 12 – 6 form. This model was first employed in two dimensions [55] and later generalized to three-dimensional AB proteins [56, 57], partially with modifications taking implicitly into account additional torsional energy contributions of each bond. The energy function for the polymer is thus given by

$$E_p = 4 \sum_{i=1}^{N-2} \sum_{j=i+2}^N (r_{ij}^{-12} - r_{ij}^{-6}) + \frac{1}{4} \sum_{i=1}^{N-2} (1 - \cos \vartheta_i). \quad (1)$$

In this work, we assume that the polymer chain interacts with an attractive spherical surface. The interaction of the polymer chain monomers and the attractive sphere is modeled by the energy

$$V_s = 4\epsilon_c \frac{\pi R_s}{r_i} \left\{ \frac{1}{5} \left[ \left( \frac{\sigma}{r_i - R_s} \right)^{10} - \left( \frac{\sigma}{r_i + R_s} \right)^{10} \right] - \frac{\epsilon}{2} \left[ \left( \frac{\sigma}{r_i - R_s} \right)^4 - \left( \frac{\sigma}{r_i + R_s} \right)^4 \right] \right\}, \quad (2)$$

where  $R_s$  is the radius of the sphere,  $r_i = (x_i^2 + y_i^2 + z_i^2)^{1/2} \geq R_s$  is the distance of a monomer to the origin and  $x_i, y_i, z_i$  are the coordinates of monomers, and  $\sigma, \epsilon_c$ , and  $\epsilon$  are set to unity. The radius of the sphere  $R_s$  is varied during the simulations. The functional dependence of the potential is shown in Fig. 1 for selected  $R_s$  values. The phenomena result from competition of intrinsic monomer-monomer and monomer-surface wall interactions. For instance in the case of adsorption of polyelectrolyte chains onto oppositely charged interfaces, the electrostatic potential controls the competition of polymer-surface adsorption-desorption behaviour.

To make contact to experimental polymer-substrate systems one may identify the empirical (dimensionful) coupling parameters of, say, the Martini force field [58] with the (dimensionless) parameters of our coarse-grained model. For instance, from Table 1 in Ref. [59] we read off that methylene has  $\epsilon_{\text{phys}} = 104 \times 8.31/1000 = 0.86\text{kJ/mol}$  which maps approximately onto  $\epsilon = 1.0$  in our model. We obtain that the 20-mer (4 methylenes per bead) discussed in our model corresponds approximately to n-C80. Similarly, the substrate maps approximately onto a polystyrene colloidal sphere, but its adsorption propensity is weaker than that of carbon or silica.

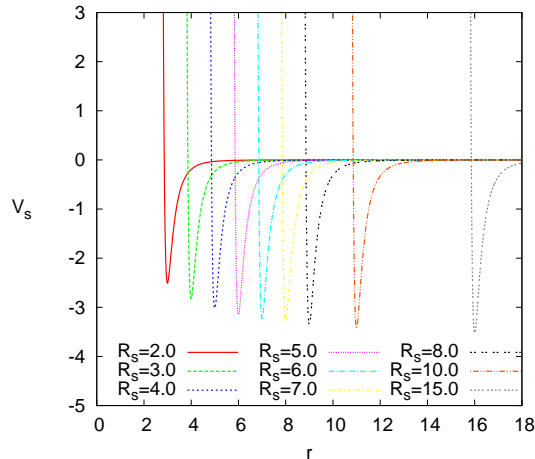


FIG. 1: The functional dependence of the attractive sphere potential (2) for different values of the sphere radius  $R_s$ .

### III. SIMULATION SETUP

#### A. Multicanonical method

In order to obtain statistical results of sufficient accuracy we applied the multicanonical Monte Carlo algorithm [60] (for reviews, see Refs. [61, 62]), where the energy distribution is flattened artificially allowing, in principle, for a random walk of successive states in energy space. This flattening is controllable and therefore reproducible. To this end, the Boltzmann probability is multiplied by a weight factor  $W(E)$ , which in our case is a function of the energy. Then the multicanonical probability for a state  $\{\mathbf{x}\}$  with energy  $E(\{\mathbf{x}\})$  reads  $p_M(E) = \exp(-E/k_B T)W(E)$ . In order to obtain a multicanonical or “flat” distribution, the initially unknown weight function  $W(E)$  has to be determined iteratively: In the beginning, the weights  $W^{(0)}(E)$  are set to unity for all energies letting the first run be a usual Metropolis simulation which yields an estimate  $H^{(0)}(E)$  for the canonical distribution. This histogram is used to determine the next guess for the weights, the simplest update is to calculate  $W^{(1)}(E) = W^{(0)}(E)/H^{(0)}(E)$ . Then the next run is performed with probabilities  $p_M^{(1)}(E) = \exp(-E/k_B T)W^{(1)}(E)$  of states with energy  $E$ , yielding  $H^{(1)}(E)$  and  $W^{(2)}(E) = W^{(1)}(E)/H^{(1)}(E)$ , and so on. The iterative procedure is continued until the weights are appropriate in a way that the multicanonical histogram  $H(E)$  is “flat”. After having determined accurate weights  $W(E)$ , they are kept fixed and following some thermalization sweeps a long production run is performed, where statistical quantities  $O$  are obtained multicanonically,  $\langle O \rangle_M = \sum_{\{\mathbf{x}\}} p_M(E(\{\mathbf{x}\}))O(\{\mathbf{x}\})/Z_M$  with the multicanonical partition function  $Z_M = \sum_{\{\mathbf{x}\}} p_M(E(\{\mathbf{x}\}))$ . The canonical statistics is obtained by reweighting the multicanonical to the canonical distribution, i.e., expectation values are computed as  $\langle O \rangle = \langle OW^{-1} \rangle_M / \langle W^{-1} \rangle_M$ . For a recent review of these methodological aspects in the context of polymer simulations, see Refs. [63, 64].

#### B. Observables

To obtain as much information as possible about the canonical equilibrium behavior, we define the following suitable quantities  $O$ . Next to the canonical expectation values  $\langle O \rangle$ , we also determine the fluctuations about these averages, as represented by the temperature derivative  $d\langle O \rangle/dT = (\langle OE \rangle - \langle O \rangle \langle E \rangle) / T^2$ . We use generic units, in which  $k_B = 1$ .

In order to identify conformational transitions, the specific heat (per monomer)  $C_V(T) = (\langle E^2 \rangle - \langle E \rangle^2) / NT^2$  with  $\langle E^k \rangle = \sum_E g(E)E^k \exp(-E/T) / \sum_E g(E) \exp(-E/T)$  is calculated from the density of states  $g(E)$ . The density of states was found (up to an unimportant overall normalization constant) by reweighting the multicanonical energy distribution obtained with multicanonical sampling to the canonical distribution. Details are given in Ref. [64].

Apart from the specific heat, several structural quantities are of interest. In order to check the structural compactness of conformations or to identify the possible dispersion of conformations because of adsorption, the radius of gyration of the conformations is calculated. The radius of gyration is a measure for the extension of the polymer and defined by  $R_g^2 \equiv \sum_{i=1}^N (\vec{r}_i - \vec{r}_{\text{cm}})^2 / N = \sum_{i=1}^N \sum_{j=1}^N (\vec{r}_i - \vec{r}_j)^2 / 2N^2$  with  $\vec{r}_{\text{cm}} = \sum_{i=1}^N \vec{r}_i / N$  being the center-of-mass of the polymer.

We also calculated various shape descriptors derived from the gyration tensor [65–68] which is defined as

$$S = \frac{1}{N} \begin{pmatrix} \sum_i (x_i - x_{\text{cm}})^2 & \sum_i (x_i - x_{\text{cm}})(y_i - y_{\text{cm}}) & \sum_i (x_i - x_{\text{cm}})(z_i - z_{\text{cm}}) \\ \sum_i (x_i - x_{\text{cm}})(y_i - y_{\text{cm}}) & \sum_i (y_i - y_{\text{cm}})^2 & \sum_i (y_i - y_{\text{cm}})(z_i - z_{\text{cm}}) \\ \sum_i (x_i - x_{\text{cm}})(z_i - z_{\text{cm}}) & \sum_i (y_i - y_{\text{cm}})(z_i - z_{\text{cm}}) & \sum_i (z_i - z_{\text{cm}})^2 \end{pmatrix}. \quad (3)$$

Transformation to the principal axis system diagonalizes  $S$ ,

$$S = \text{diag}(\lambda_1, \lambda_2, \lambda_3), \quad (4)$$

where we assume that the eigenvalues of  $S$  are sorted in descending order, i.e.,  $\lambda_1 \geq \lambda_2 \geq \lambda_3$ . The first invariant of  $S$  gives the squared radius of gyration,

$$\text{Tr } S = \lambda_1 + \lambda_2 + \lambda_3 = R_g^2, \quad (5)$$

which agrees with the definition given above. The second invariant shape descriptor, or relative shape anisotropy, is defined as

$$\kappa^2 \equiv A_3 = \frac{3}{2} \frac{\text{Tr } \hat{S}^2}{(\text{Tr } S)^2} = 1 - 3 \frac{\lambda_1 \lambda_2 + \lambda_2 \lambda_3 + \lambda_3 \lambda_1}{(\lambda_1 + \lambda_2 + \lambda_3)^2}, \quad (6)$$

where  $\hat{S} = S - \frac{1}{3}(\text{Tr } S)E$  with unit tensor  $E$ . It reflects both the symmetry and dimensionality of a polymer conformation. This parameter is limited between the values of 0 and 1. It reaches 1 for an ideal linear chain and drops to zero for highly symmetric conformations. For planar symmetric objects, the relative shape anisotropy converges to the value of 1/4 [65–69].

The distance of the center-of-mass,  $r_{\text{cm}}$ , of the polymer to the surface also provides clear evidence that the polymer is freely moving or that it is very close to the surface and just adsorbed. Another useful quantity is the mean number of monomers  $\langle N_s \rangle$  docked to the surface. A single-layer structure is formed if all monomers are attached at the sphere; if none is attached, the polymer is desorbed. The sphere potential is a continuous potential, and in order to distinguish monomers docked to the sphere from those not being docked, it is reasonable to introduce a cutoff. We define a monomer  $i$  as being “docked” if  $r_i - R_s < r_c \equiv 1.2$ . The corresponding measured quantity is the average number  $\langle N_s \rangle$  of monomers docked to the surface. This can be expressed as  $N_s = \sum_{i=1}^N \Theta(r_c - r_i)$ , where  $\Theta(r)$  is the Heaviside step function.

### C. Computational details

In our simulations, the polymer chain length is  $N = 20$  and we set  $\epsilon = 1.0$  large enough to allow adsorption of the polymer to the sphere surface. We consider two different situations, one is the case where the polymer is grafted with one end to the substrate and in the second case it is allowed to move freely in the space above the substrate over a distance  $L = 60 - R_s$  from the sphere surface (i.e., the nano-sphere of radius  $R_s$  is centered in a spherical container of radius 60 with a purely steric wall), which is called the free or non-grafted case. We have done simulations with different sizes of the sphere. The random initial configurations for the non-grafted and grafted cases of the simulation are sketched in Figs. 2(a) and (b). The total energy of the system is composed of the pure polymer chain energy and the polymer chain attractive sphere interaction energy. The initial configuration of the polymer chain is randomly generated. For the determination of the multicanonical weights we performed 200 iterations with at least  $10^5$  sweeps each. In the production period,  $1 \times 10^8$  sweeps were generated to have reasonable statistics for estimating the thermodynamic quantities. Statistical errors are estimated with the standard Jackknife technique [70–72].

## IV. RESULTS

### A. Energetic fluctuations

In Fig. 3 the specific-heat curves  $C_V(T)$  as a function of temperature  $T$  for different values of sphere radius  $R_s$  are displayed for the (a) non-grafted and (b) end-grafted case. In both cases the specific heat shows two transitions: one is the low-temperature transition which is almost at the same temperature for all different  $R_s$  values. This is the freezing transition. Even though this transition occurs at the same temperature, the conformations have different

characteristic shapes depending on the attraction strength of the sphere. For describing these different shapes we will concentrate on structural observables to be discussed below. The second transition has only a weak signal for the grafted case (a shoulder at  $T \approx 2.0$ ) but for the non-grafted case it is quite pronounced. This is the adsorption transition, which comes into play at higher temperatures than the freezing transition and depends on the sphere radius. Increasing the sphere radius causes also an increase in the adsorption transition temperature. This transition separates desorbed (D) and adsorbed (A) conformations.

## B. Phase diagram

The phase structure derived from all of our observables is summarized by the phase diagrams in the  $R_s - T$  plane given in Fig. 4 for the (a) non-grafted and (b) end-grafted case. Representative conformations that predominate in the different structural phases of a non-grafted polymer are revealed in Fig. 5. The phase diagram is constructed by combining all the informations coming from the canonical expectation values of our observables and their temperature derivatives. Some of our observables exhibit a peak at all of the transitions in the phase diagram, while others are only sensitive to one of them. For example, the collapse transition line is seen quite clearly from the peak in the temperature derivative of the canonical expectation value of the eigenvalues of the gyration tensor and from the radius of gyration. On the other hand, the adsorption line is most clearly built up by the mean number of adsorbed monomers to the surface and by the distance of the center-of-mass of the polymer to the substrate. Since our system is a finite system, it is not possible to determine the transition lines precisely: The transition lines still vary with chain length  $N$  and the observables have broad peaks. Thus we have a certain band width which approximately covers the different peaks in the observables.

In the phase diagram the temperature increases from bottom to top and the radius of the sphere increases from left to right. The boundaries separate the individual conformational phases. For small sphere radius  $R_s$ , the polymer behaves similarly to a free polymer where at high temperatures the typical conformations are desorbed and extended or random coil. Decreasing the temperature causes the collapse transition into globular conformations which are still in the desorbed phase. But below the freezing transition all the compact conformations are adsorbed. At this point, for the grafted case all the conformations are already adsorbed below the collapse transition. There is no desorbed globule phase in the grafted phase diagram. One more difference occurred also in the high-temperature desorbed phase. In the non-grafted case some structural observables give indication for some changes in the desorbed



FIG. 2: (Color online) Start configurations of the simulations: (a) non-grafted, (b) end-grafted. The polymer chain length is  $N = 20$  and we set  $\epsilon = 1.0$  in our simulations.

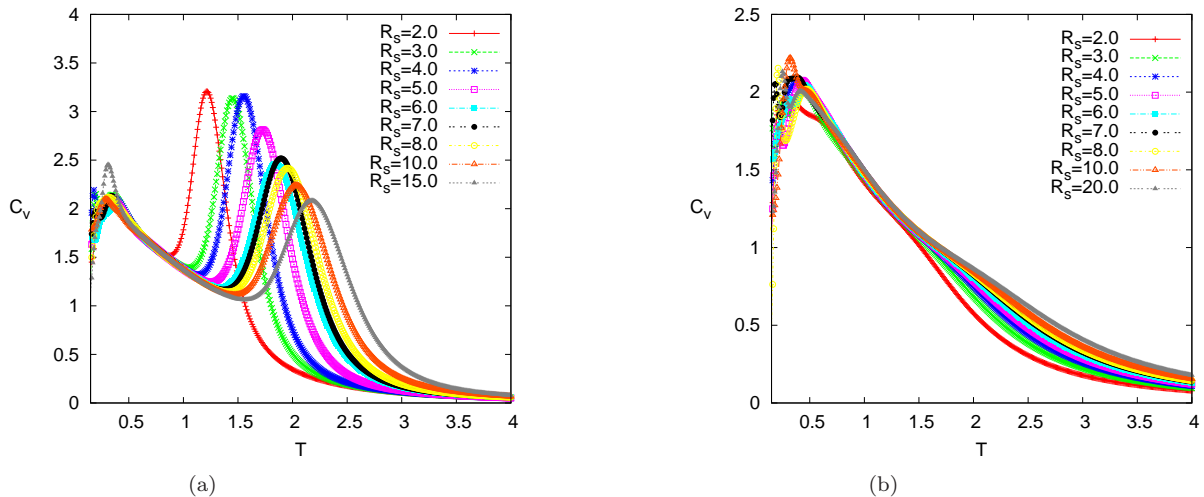


FIG. 3: (Color online) Specific heat as a function of temperature for different sphere radii  $R_s$  for the (a) non-grafted and (b) end-grafted case. The polymer chain length is  $N = 20$  and we set  $\epsilon = 1.0$  in our simulations.

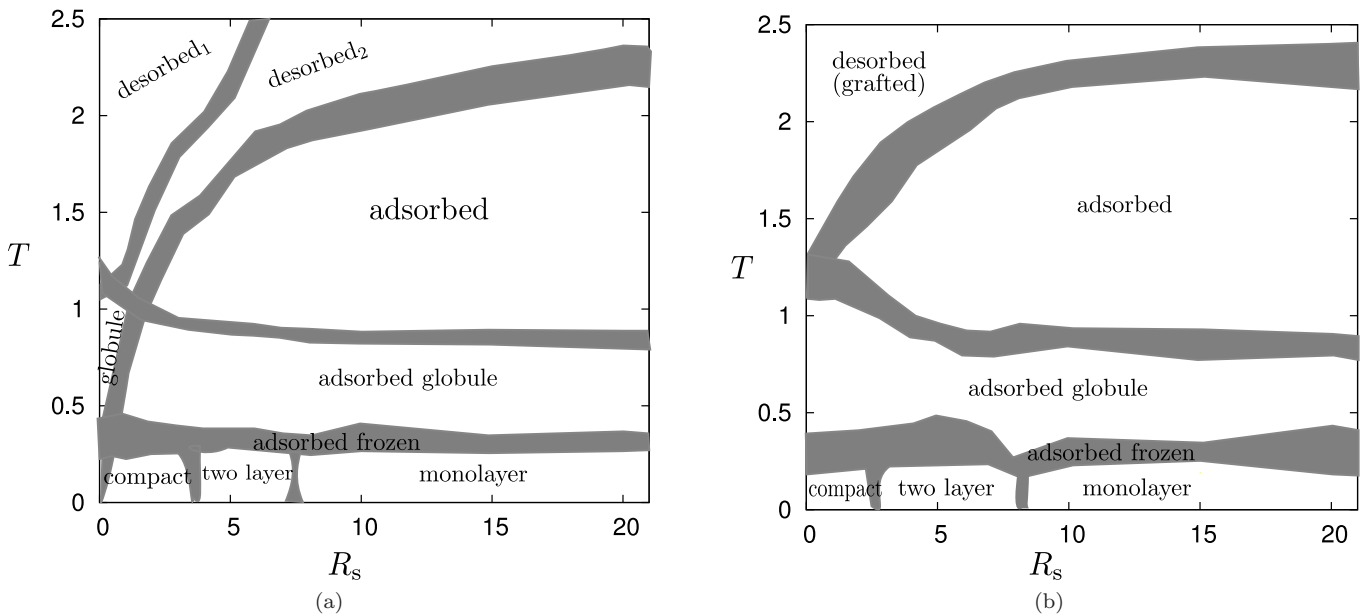


FIG. 4: The phase diagram of the homopolymer-attractive spherical surface system for a (a) non-grafted and (b) end-grafted polymer as obtained in extensive multicanonical simulations. The boundaries separate the individual conformational phases. The band width shows the variation of the peaks of temperature derivatives of different structural observables which have been analyzed simultaneously. In our simulations, the polymer chain length is  $N = 20$  and we set  $\epsilon = 1.0$  for the representation of attractive surface.

phase. When we detect carefully the conformations we see that those in the “desorbed<sub>1</sub>” phase are far away from the sphere surface while the conformations in the “desorbed<sub>2</sub>” phase are almost adsorbed. Thus they feel very strongly the surface effect. Because of the grafting, this is not the case for a grafted polymer. Increasing the sphere radius approximately to  $R_s = 7.0$  leads to very fast increase in the adsorption transition temperature, but after this value it increases slowly. The adsorption transition separates the regions of desorbed and adsorbed phases. Besides the collapse, adsorption, and freezing transitions, the most pronounced transition is the layering transition which occurs at  $R_s \approx 7.0$  and separates the region of planar conformations which are monolayers and totally adsorbed conformations from the two-layer and compact conformations.

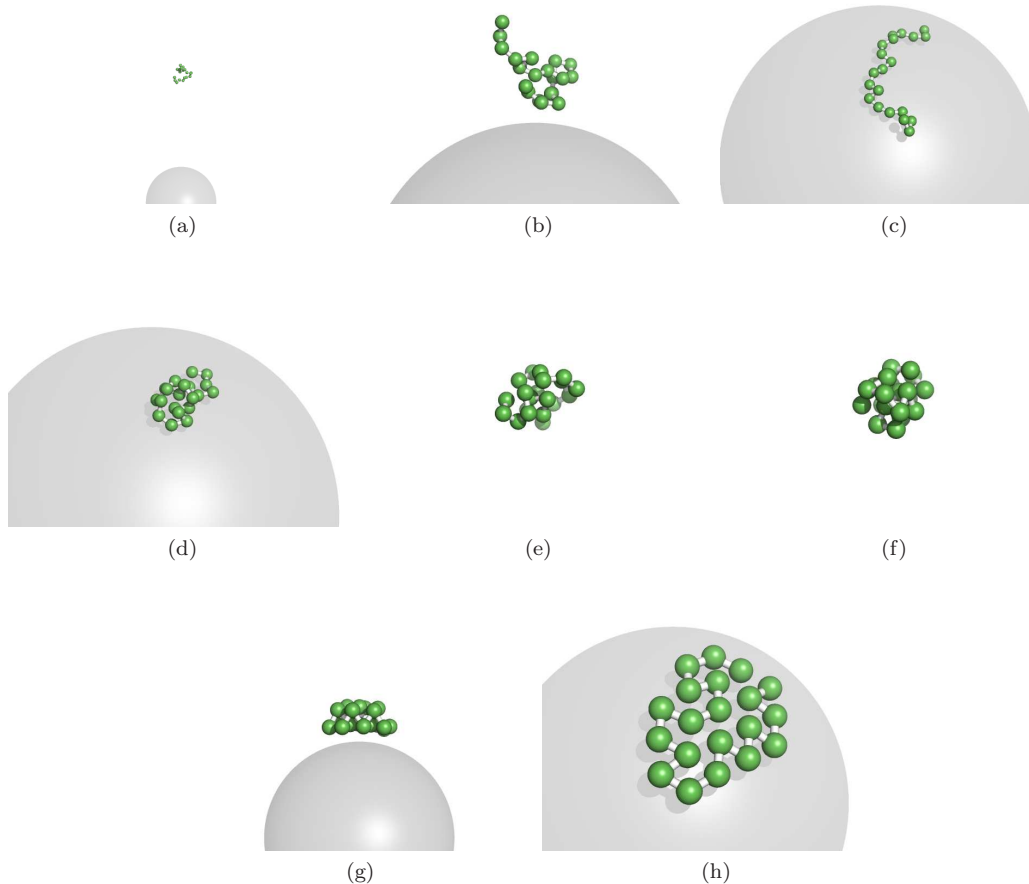


FIG. 5: (Color online) Typical conformations for the regions (a) desorbed<sub>1</sub>, (b) desorbed<sub>2</sub>, (c) adsorbed, (d) adsorbed globule, (e) globule, (f) compact, (g) two layer, and (h) monolayer in the phase diagram for a non-grafted polymer.

In the following discussion we will mainly focus on the non-grafted polymer and display the findings from the structural observables in detail only for this case. However, since the phase diagrams in Figs. 4(a) and (b) rely on these data, we have measured and analyzed all these observables for the grafted case, too, and hence shall give at least an overview of the analogous results in a panel of figures at the end of this section, but refrain from a detailed description.

### C. Structural parameters and fluctuations

In Figs. 6(a) non-grafted and (b) end-grafted cases, The radius of gyration  $\langle R_g \rangle$  as a function of temperature for the non-grafted and end-grafted cases are given in Figs. 6(a) and (b) respectively. We have also present the temperature derivative  $d\langle R_g \rangle/dT$  for different values of the sphere radius  $R_s$  in Figs. 6(c) and (d) for both cases. For small values of  $R_s$ ,  $R_s = 0.5, 1.0$ , the most compact conformations occur in the low-temperature region with an average  $\langle R_g \rangle \approx 1.23$  (data not shown). Slightly increasing the  $R_s$  value causes also an increase in the average  $\langle R_g \rangle$  value to about 1.4. Increasing the  $R_s$  parameter further, the curve at  $R_s = 7.0$  has a minimum behavior at low temperatures. As a function of temperature the radius of gyration is monotonically increasing for all  $R_s$  values except beyond  $R_s = 7.0$  where the layering transition occurs. Same supporting informations are also gained from the relative shape anisotropy parameter which is shown in Fig. 7.

If we consider now the temperature derivative given in Fig. 6(c), we detect two peaks. The peak in the temperature derivative of the canonical expectation value of radius of gyration at low temperatures indicates the collapse transition quite clearly. Also its tensor eigenvalues [Figs. 10(a) and (b) below and particularly the relative shape anisotropy parameter  $\langle \kappa^2 \rangle$  in Figs. 7(a) and (b), which is the second invariant of the tensor, give rich information and support

our findings. As we discussed before the desorbed phase is divided into two regions which are called “desorbed<sub>1</sub>” and “desorbed<sub>2</sub>”. The boundary of these regions is emerging in the temperature derivative of radius of gyration  $d\langle R_g \rangle/dT$  and in the temperature derivative of the relative shape anisotropy  $d\langle \kappa^2 \rangle/dT$  as a second peak at high temperatures, since the peaks are going to become invisible with increasing  $R_s$  values and also are smaller than the peaks at low temperatures. We have investigated the conformations in both regions in detail and concluded that the conformations in the “desorbed<sub>1</sub>” phase are far away from the surface. On the other hand, the conformations in the “desorbed<sub>2</sub>” phase are almost adsorbed to the sphere boundary, which indicates the influence of the surface on the desorbed phase.

The adsorption transition can best be detected by the distance of the center-of-mass of the polymer to the substrate  $r_{\text{cm}}$  and by the mean number of adsorbed monomers, where a monomer is defined to be adsorbed to the surface if  $r_i - R_s < 1.2$ . The behavior of these two observables, in particular the peaks in their temperature derivatives, build the adsorption line in the phase diagrams. In Figs. 8(a) and (b) the distance of the center-of-mass of the polymer to the substrate and its temperature derivative are given, respectively. As can be seen in the figure, for large temperatures the polymer can move freely within the simulation space and the influence of the surface is minimal only for high  $R_s$  values, whereas for low  $R_s$  the influence is purely steric. Thus, the average center-of-mass distance of the polymer above the surface is nearly half of the simulation space. On contrary, at low temperatures the polymer favors surface contacts and the average center-of-mass distance converges to the minimum location of the potential (cf. Fig. 1). One clearly detects a quite pronounced peak in its temperature derivative [Fig. 8(b)] that divides the phase space into adsorbed and desorbed phases. Consistently with our discussion above, the pronounced tendency of the polymer to make surface contacts can be also identified from the mean number of adsorbed monomers to the surface  $\langle N_s \rangle$  [Fig. 9(a)] and the negative minima in its temperature derivative [Fig. 9(b)]. They are in good agreement with the sharp peaks in the temperature derivative of the distance of the center-of-mass of the polymer which together draws the adsorption line in the phase diagram.

Finally, the eigenvalues of the gyration tensor which measure the extensions in the principle axis system are extracted to complement the picture. In Figs. 10(a)-(f) the eigenvalues of the gyration tensor and their fluctuations as a function of temperature  $T$  for different values of  $R_s$  are displayed. They all support our earlier findings. But the most important result deductible from the eigenvalues is that: The third eigenvalue of the gyration tensor  $\langle \lambda_3 \rangle$  converges to small values which means that the extension in the third direction vanishes and the conformations are two-dimensional signaling the layering transition. To support this finding one can also plot the ratio of the largest eigenvalue to the smallest eigenvalue  $\langle \lambda_1/\lambda_3 \rangle$  and its temperature derivative as in Fig. 11. This ratio assumes small values until  $R_s \approx 7.0$ . Above  $R_s = 7.0$  the ratio of the eigenvalues jumps to much higher values, signaling that the layering transition occurs at this  $R_s$  value and separates the conformational space from planar conformations.

#### D. Grafted case

Finally, for comparison we show for the grafted case in Figs. 12(a)-(h) the analogs to Figs. 6-9. These results are used when constructing the phase diagram for an end-grafted polymer in Fig. 4(b). By comparing this set of plots with the free case, the most important outcome is that: A crossover occurs from low temperature, where the polymer is adsorbed and the conformations of a grafted polymer and a free polymer are very similar, to high temperatures, where the free polymer approaches the behavior of a polymer in bulk solution while that of a grafted polymer is always affected by the attractive sphere surface. Because of this effect, the transition is just a crossover which can be clearly seen in the  $\langle r_{\text{cm}} \rangle$  and  $\langle N_s \rangle$  parameters. In the free case these parameters change sharply because as soon as the polymer desorbs, it leaves the influence of the surface field. A grafted polymer, on the other hand, cannot leave the surface field. The freezing transition, however, signaled by the low-temperature peak in the specific heat displayed in Fig. 3(b), does not differ much for grafted and non-grafted chains.

#### V. CONCLUSION

In this paper, we have performed generalized-ensemble Monte Carlo computer simulations in order to investigate the full conformational behavior of a coarse-grained semiflexible finite polymer chain near an attractive spherical surface. In a systematic analysis, over a wide range of sphere radius  $R_s$  and temperature  $T$ , we have constructed the phase diagrams both for non-grafted and end-grafted polymers. For the identification of the conformational phases, we have examined several energetic and structural observables and their fluctuations by canonical statistical analysis. The transition lines in the phase diagram show the best match of all observables analyzed simultaneously in our study. In the thermodynamic limit of infinitely long chains the transitions are expected to occur at sharp values of the parameters. For finite chains, the transition lines still vary with chain length  $N$  and are not well defined because of broad peaks in the observables that also have small differences in between. Therefore the locations of the phase

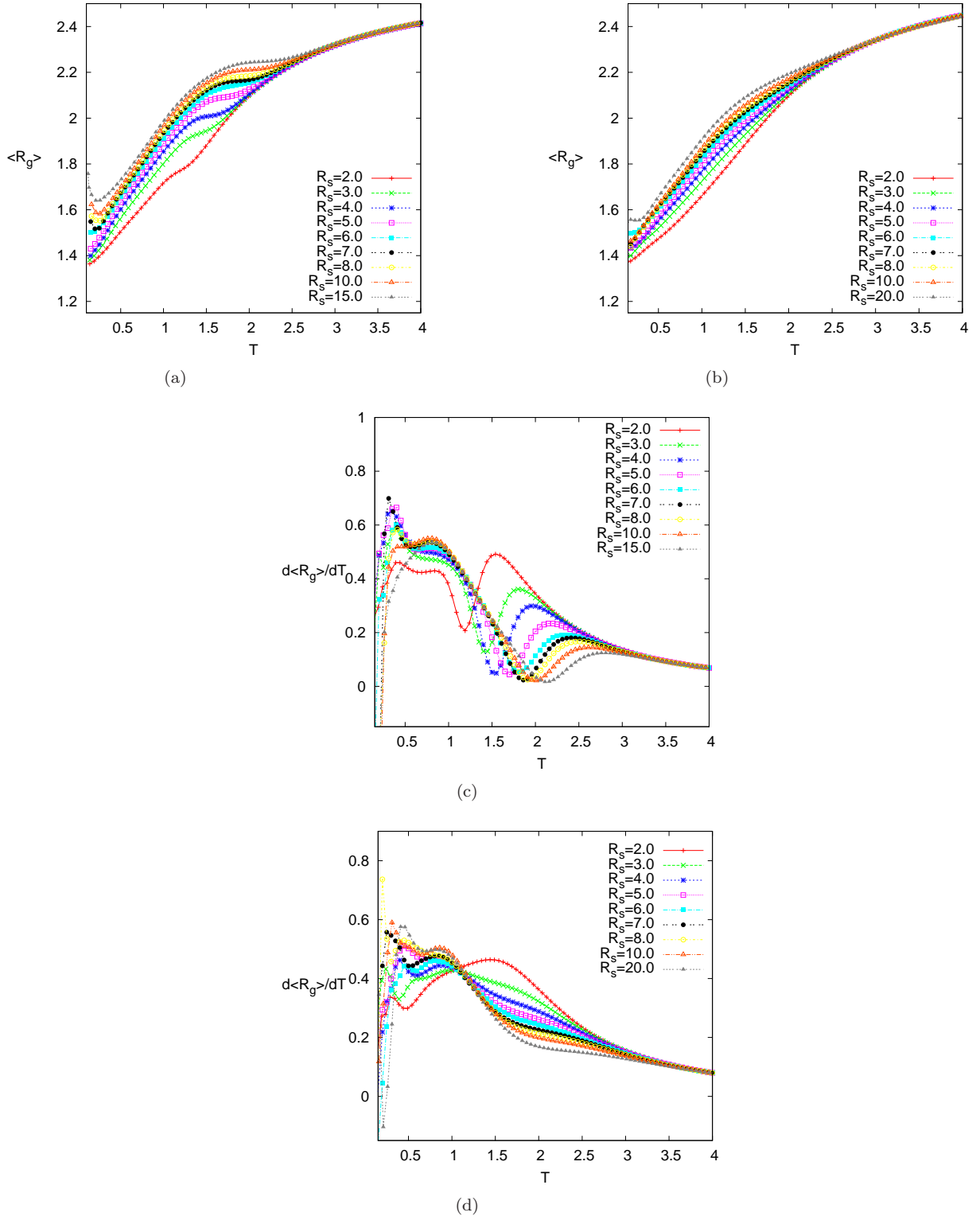


FIG. 6: (Color online) (a) The canonical expectation value of the radius of gyration  $\langle R_g \rangle$  for non-grafted (b) end-grafted and its temperature derivative for different sphere radii  $R_s$  (c) for non-grafted (d) end-grafted cases. In our simulations, the polymer chain length is  $N = 20$  and we set  $\epsilon = 1.0$  for the representation of attractive surface.

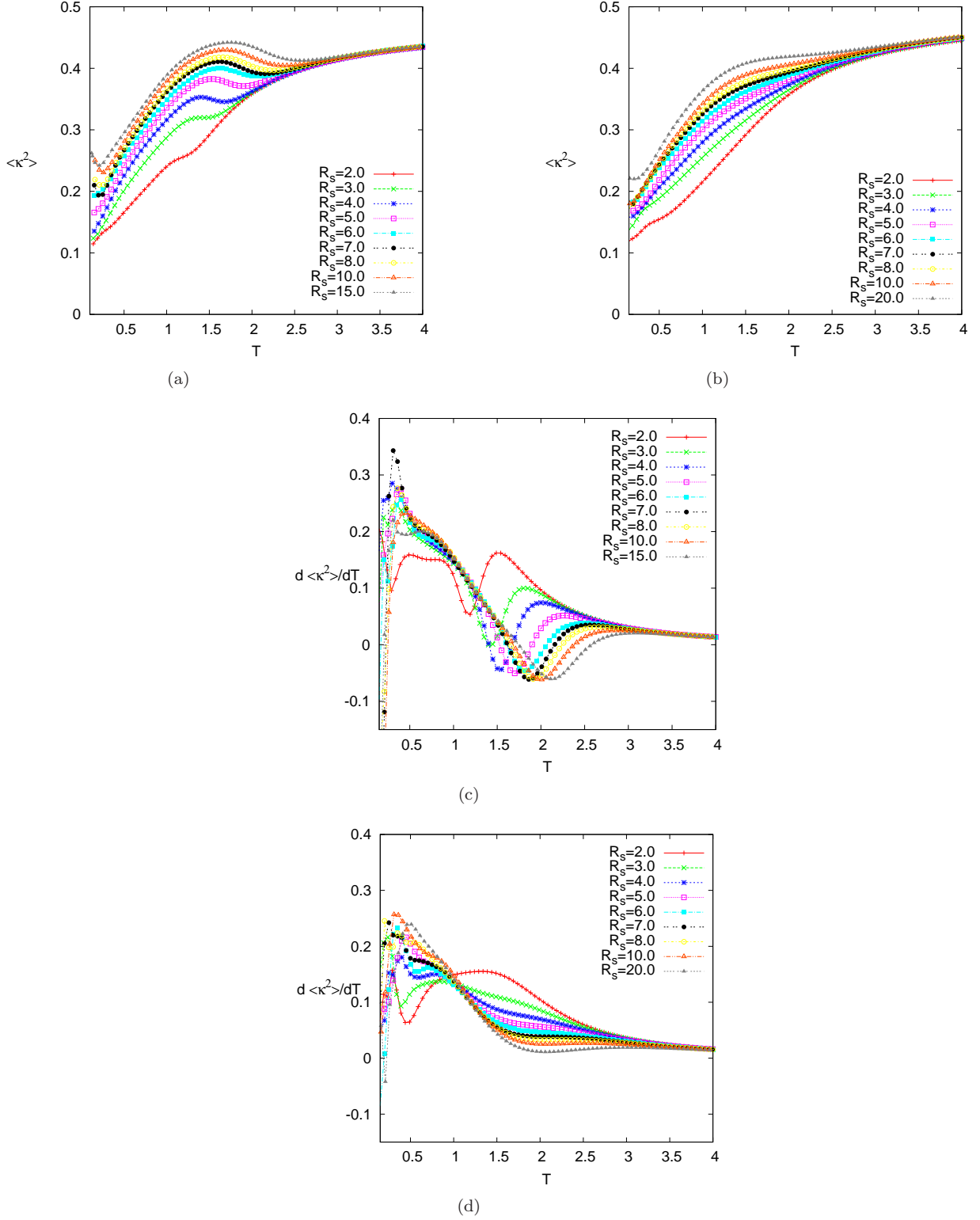


FIG. 7: (Color online) The canonical expectation value of the relative shape anisotropy parameter  $\langle \kappa^2 \rangle$  for (a) non-grafted (b) for end-grafted and its temperature derivative for different sphere radii  $R_s$  for (c) non-grafted (d) for end-grafted cases. In our simulations, the polymer chain length is  $N = 20$  and we set  $\epsilon = 1.0$  for the representation of attractive surface.

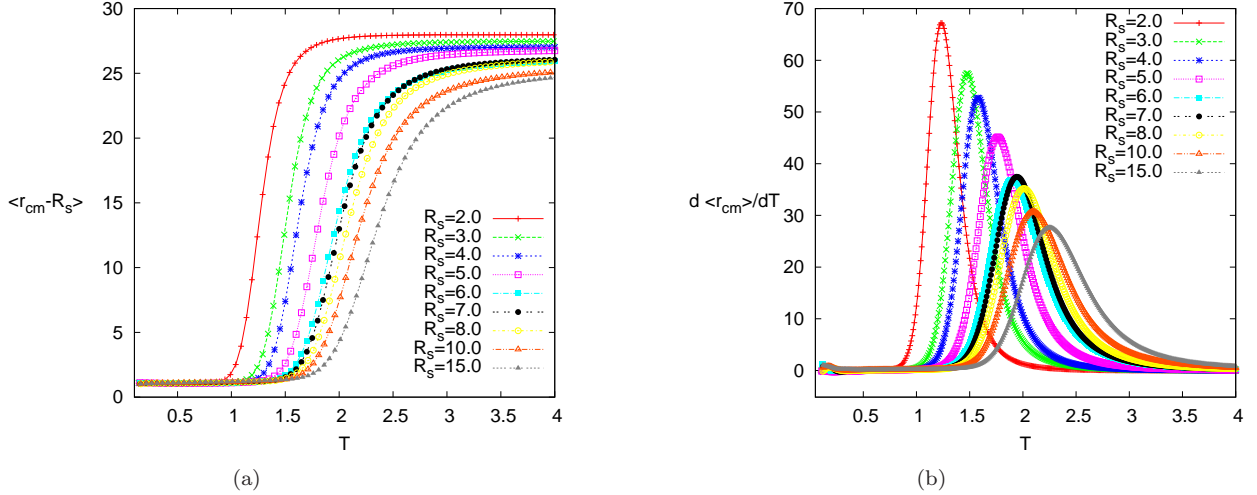


FIG. 8: (Color online) (a) The canonical expectation value of the distance of the center-of-mass of the polymer  $\langle r_{cm} \rangle$  from the sphere surface and (b) its temperature derivative for different sphere radii  $R_s$ . In our simulations, the polymer chain length is  $N = 20$  and we set  $\epsilon = 1.0$  for the representation of attractive surface.

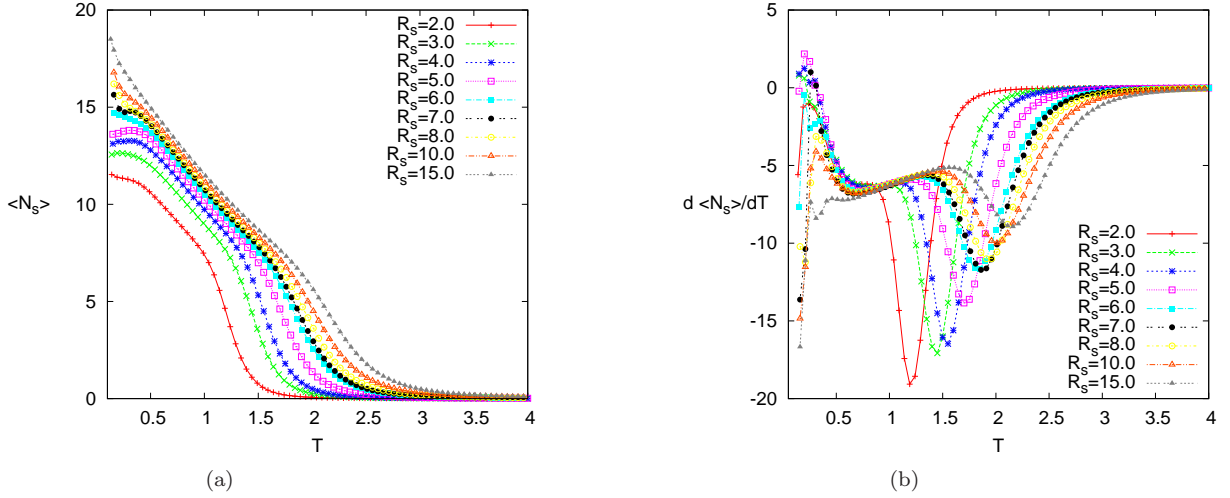


FIG. 9: (Color online) (a) The canonical expectation value of the mean number of docked monomers  $\langle N_s \rangle$  and (b) its temperature derivative for different sphere radii  $R_s$ . In our simulations, the polymer chain length is  $N = 20$  and we set  $\epsilon = 1.0$  for the representation of attractive surface.

boundaries should be considered as a rough guide. However, even for the rather short chains considered here, we can clearly identify different phases which show distinguishing features, so that a reasonable picture is obtained. Most of the phases are believed to still persist for longer chains. All our results obtained from the different observables are summarized in the phase diagrams in the  $R_s - T$  plane which for a convenient overview were already displayed earlier in Figs. 4(a) for non-grafted and (b) for end-grafted polymers. Their typical conformations were also revealed already earlier in Fig. 5. To summarize these findings, we give in the following a short description of each phase:

**Desorbed<sub>1</sub>:** Random coil structures with no surface contacts. These conformations freely circulate in the simulation space and are far away from the surface [Fig. 5(a)].

**Desorbed<sub>2</sub>:** Desorbed conformations, but they are almost adsorbed. The conformations feel the influence of the surface [Fig. 5(b)].

**Adsorbed:** Partially adsorbed, extended conformations [Fig. 5(c)].

**Adsorbed Globule:** Partially adsorbed conformations [Fig. 5(d)].

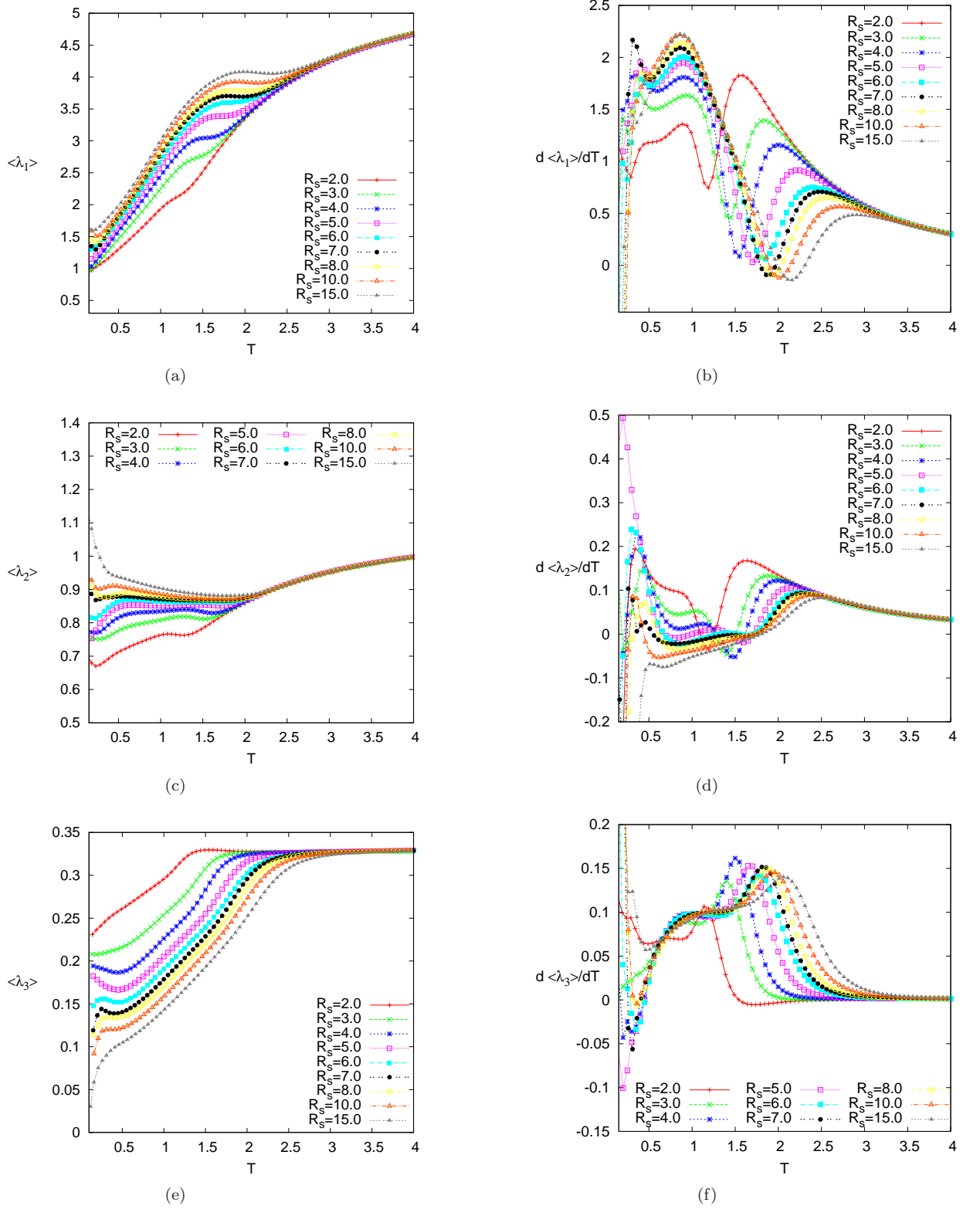


FIG. 10: (Color online) The canonical expectation values of the three eigenvalues  $\langle \lambda_1 \rangle$ ,  $\langle \lambda_2 \rangle$ , and  $\langle \lambda_3 \rangle$  of the gyration tensor and their temperature derivatives for different sphere radii  $R_s$ . In our simulations, the polymer chain length is  $N = 20$  and we set  $\epsilon = 1.0$  for the representation of attractive surface.

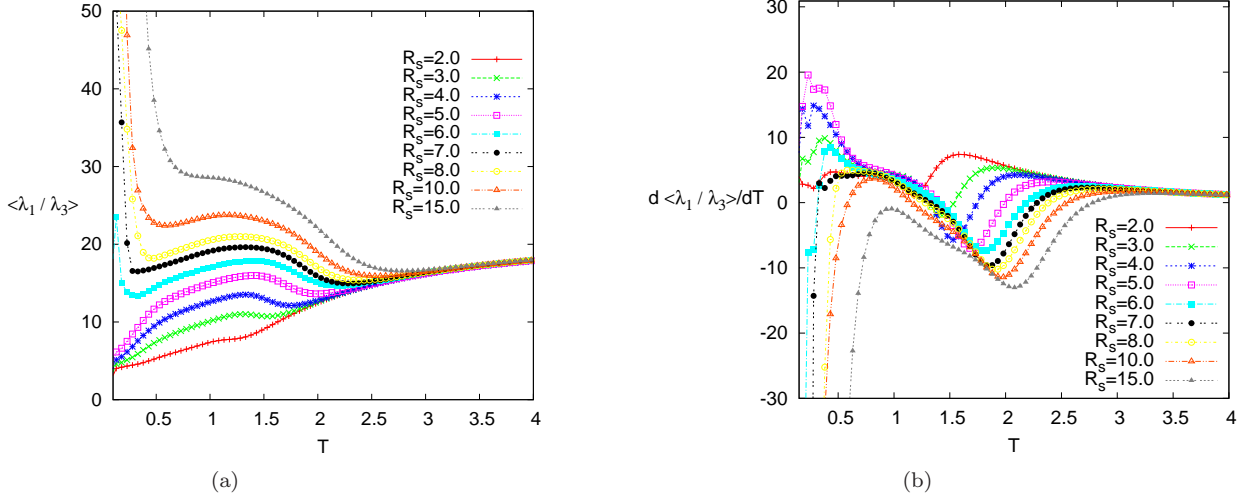


FIG. 11: (Color online) (a) The ratio of the largest eigenvalue to the smallest eigenvalue  $\langle \lambda_1 / \lambda_3 \rangle$  and (b) its temperature derivative for different sphere radii  $R_s$ . In our simulations, the polymer chain length is  $N = 20$  and we set  $\epsilon = 1.0$  for the representation of attractive surface.

**Globule:** Desorbed globule conformations. These conformations are only seen on the non-grafted phase diagram [Fig. 5(e)].

**Compact:** Partially adsorbed, globular conformations like a drop on the wall of the sphere [Fig. 5(f)].

**Two Layer:** Partially adsorbed, compact conformations. These are two-layer structures. The lower layer of the conformations is adsorbed and lies on the wall of the sphere [Fig. 5(g)].

**Monolayer:** Completely adsorbed, compact conformations. These single-layer structures lie on the surface of the sphere and fit the sphere wall perfectly [Fig. 5(h)].

It is clear that, for longer chains, the desorbed, globule and compact phases obviously will survive. Additionally, filmlike (monolayer) and semispherical conformations (two layer), as well as surface attached globular shapes will dominate the respective phases. On the other hand, as long as surface effects are as influential as volume effects the compact adsorbed conformations differ noticeably for polymers with different but small lengths. But, for the majority of phases we find qualitative coincidence with a simple coarse-grained model.

In addition to experimental results [73, 74], Feng and Ruckenstein [34] examined the adsorption of a polyampholyte chain on a single spherical nano-particle with three different radii of the particles. There, the charge density at the particle surface regulates the strength of the adsorption field and the polymer composition regulates the location of the coil-globule transition. In this study, we kept the adsorption field constant (whereas we varied the adsorption strength in another earlier study) and varied the radius of the nano-particles and observed qualitatively the described scenarios. As a result, our model system can be mapped in the considered parameter range to a real system considered in experiments. Comparing with experimental findings, computational studies have the advantage that different combinations of parameters can be varied at will over long ranges and a deeper knowledge starting from the origin can be extracted.

## ACKNOWLEDGMENTS

We wish to thank Viktoria Blavatska and Bernd Abel for useful discussions. H.A. acknowledges support by the Alexander von Humboldt Foundation under the Experienced Researcher Fellowship Programme. W.J. thanks the German Research Foundation (DFG) for support under Grant Nos. JA483/24-3 and SFB/TRR 102 (Project B04). We also benefitted from the Marie Curie IRSES network DIONICOS under Contract No. PIRSES-GA-2013-612707 within the European Union Seventh Framework Programme. The computer time for the Monte Carlo simulations

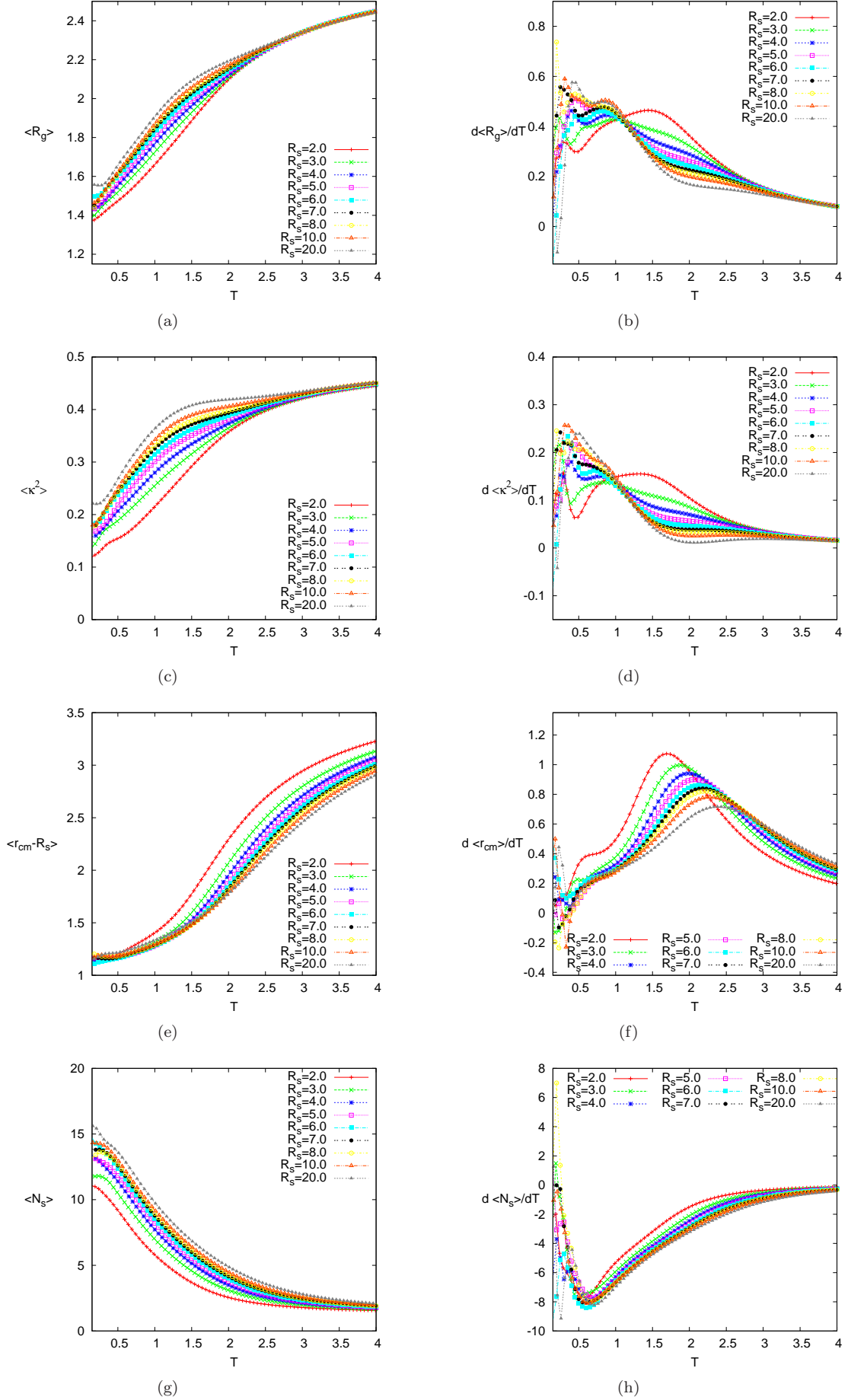


FIG. 12: (Color online) Same observables as in Figs. 6-9 but here for the end-grafted case. In our simulations, the polymer chain length is  $N = 20$  and we set  $\epsilon = 1.0$  for the representation of attractive surface.

was provided by NIC, Forschungszentrum Jülich, under Grant No. hlz21, which we gratefully acknowledge.

- 
- [1] R. F. Service, *Science* **270**, 230 (1995).
- [2] S. Walheim, E. Schaffer, J. Mlynek, and U. Steiner, *Science* **283**, 520 (1999).
- [3] S. Brown, *Nature Biotechnol.* **15**, 269 (1997).
- [4] R. Braun, M. Sarikaya, and K. Schulten, *J. Biomater. Sci. Polymer Edn.* **13**, 747 (2002).
- [5] S. R. Whaley, D. S. English, E. L. Hu, P. F. Barbara, and A. M. Belcher, *Nature* **405**, 665 (2000).
- [6] K. Goede, P. Busch, and M. Grundmann, *Nano Lett.* **4**, 2115 (2004).
- [7] M. Bachmann, K. Goede, A. G. Beck-Sickinger, M. Grundmann, A. Irbäck, and W. Janke, *Angew. Chem. Int. Ed.* **49**, 9530 (2010).
- [8] E. Eisenriegler, K. Kremer, and K. Binder, *J. Chem. Phys.* **77**, 6296 (1982).
- [9] R. Descas, J.-U. Sommer, and A. Blumen, *J. Chem. Phys.* **120**, 8831 (2004).
- [10] M. Bachmann and W. Janke, *Phys. Rev. Lett.* **95**, 058102 (2005).
- [11] M. Bachmann and W. Janke, *Phys. Rev. E* **73**, 020901(R) (2006).
- [12] M. Bachmann and W. Janke, *Phys. Rev. E* **73**, 041802 (2006).
- [13] J. Luettmer-Strathmann, F. Rampf, W. Paul, and K. Binder, *J. Chem. Phys.* **128**, 064903 (2008).
- [14] M. Bachmann and W. Janke, in: *Rugged Free Energy Landscapes: Common Computational Approaches to Spin Glasses, Structural Glasses and Biological Macromolecules*, ed. W. Janke, *Lect. Notes Phys.* **736** (Springer, Berlin, 2008); pp. 203–246.
- [15] M. Möddel, M. Bachmann, and W. Janke, *J. Phys. Chem. B* **113**, 3314 (2009).
- [16] V. A. Ivanov, J. A. Martemyanova, M. Müller, W. Paul, and K. Binder, *J. Phys. Chem. B* **113**, 3653 (2009).
- [17] T. Chen, L. Wang, X. Lin, Y. Liu, and H. Liang, *J. Chem. Phys.* **130**, 244905 (2009).
- [18] L. Wang, T. Chen, X. Lin, Y. Liu, and H. Liang, *J. Chem. Phys.* **131**, 244902 (2009).
- [19] A. D. Swetnam and M. P. Allen, *Phys. Chem. Chem. Phys.* **11**, 2046 (2009).
- [20] M. Möddel, W. Janke, and M. Bachmann, *Phys. Chem. Chem. Phys.* **12**, 11548 (2010).
- [21] M. Möddel, W. Janke, and M. Bachmann, *Macromolecules* **44**, 9013 (2011).
- [22] Y. W. Li, T. Wüst, and D. P. Landau, *Phys. Rev. E* **87**, 012706 (2013).
- [23] M. Möddel, W. Janke, and M. Bachmann, *Phys. Rev. Lett.* **112**, 148303 (2014).
- [24] M. P. Taylor and J. Luettmer-Strathmann, *J. Chem. Phys.* **141**, 204906 (2014).
- [25] J. Krawczyk, A. L. Owczarek, T. Prellberg, and A. Rechnitzer, *J. Stat. Mech.: Theory Exp.*, P05008 (2005).
- [26] S. Bhattacharya, V. G. Rostiashvili, A. Milchev, and T. A. Vilgis, *Phys. Rev. E* **79**, 030802(R) (2009).
- [27] M. J. Russell, *Science* **302**, 580 (2003).
- [28] M. Lundqvist, P. Nygren, B.-H. Jonsson, and K. Broo, *Angew. Chem. Int. Ed.* **45**, 8169 (2006).
- [29] I. Gurevitch and S. Srebnik, *Chem. Phys. Lett.* **444**, 96 (2007); *J. Chem. Phys.* **128**, 144901 (2008).
- [30] T. Vogel and M. Bachmann, *Phys. Rev. Lett.* **104**, 198302 (2010).
- [31] T. Vogel, J. Gross, and M. Bachmann, *J. Chem. Phys.* **142**, 104901 (2015).
- [32] R. R. Netz and J. F. Joanny, *Macromolecules* **31**, 5123 (1998).
- [33] M. Tanaka, A. Yu Grosberg, and T. Tanaka, *J. Chem. Phys.* **110**, 8176 (1999); M. Tanaka and T. Tanaka, *Phys. Rev. E* **62**, 3803 (2000).
- [34] J. Feng and E. Ruckenstein, *Polymer* **44**, 3141 (2003).
- [35] M. Tagliazucchi, M. Olvera de la Cruz, and I. Szleifer, *Proc. Natl. Acad. Sci. U.S.A.* **107**, 5300 (2010).
- [36] S. A. Barr and A. Z. Panagiotopoulos, *J. Chem. Phys.* **137**, 144704 (2012).
- [37] A. Gladytz, M. Wagner, T. Häupl, C. Elsner, and B. Abel, *Part. Part. Syst. Char.* **32**, 573 (2015).
- [38] C. Elsner, D. Hintzen, A. Prager, K. R. Siefertmann, and B. Abel, *Z. Phys. Chem.* **229**, 427 (2015).
- [39] J. Wang and M. Muthukumar, *J. Chem. Phys.* **135** 194901 (2011).
- [40] J. McNamara, C. Y. Kong and M. Muthukumar, *J. Chem. Phys.* **117** 5354 (2002).
- [41] R. Messina, *Macromolecules* **37** (2), 621 (2004).
- [42] A. V. Dobrynin, *Curr. Opin. in Colloid and Interface Sci.* **13** 376 (2008).
- [43] A. V. Dobrynin and Mi. Rubinstein, *Prog. Polym. Sci.* **30** 1049 (2005).
- [44] R. R. Netz and D. Andelman, *Phys. Rep.* **380** 1 (2003).
- [45] R. R. Netz and J. Joanny, *Macromolecules* **32** 9013 (1999).
- [46] M. Marenz, J. Zierenberg, H. Arkin, and W. Janke, *Condens. Matter Phys.* **15**, 43008 (2012).
- [47] H. Arkin and W. Janke, *Phys. Rev. E* **85**, 051802 (2012).
- [48] H. Arkin and W. Janke, *J. Chem. Phys.* **138**, 054904 (2013).
- [49] H. Arkin and W. Janke, *J. Phys. Chem. B* **116**, 10379 (2012).
- [50] H. Arkin and W. Janke, *Eur. Phys. J. – Special Topics* **216**, 181 (2013).
- [51] T. Bogner, A. Degenhard, and F. Schmid, *Phys. Rev. Lett.* **93**, 268108 (2004).
- [52] E. Balog, T. Becker, M. Oettl, R. Lechner, R. Daniel, J. Finney, and J. C. Smith, *Phys. Rev. Lett.* **93**, 028103 (2004).
- [53] M. Ikeguchi, J. Ueno, M. Sato, and A. Kidera, *Phys. Rev. Lett.* **94**, 078102 (2005).
- [54] N. Gupta and A. Irbäck, *J. Chem. Phys.* **120**, 3983 (2004).

- [55] F. H. Stillinger, T. Head-Gordon, and C. L. Hirshfeld, *Phys. Rev. E* **48**, 1469 (1993); F. H. Stillinger and T. Head-Gordon, *Phys. Rev. E* **52**, 2872 (1995).
- [56] A. Irbäck, C. Peterson, F. Potthast, and O. Sommelius, *J. Chem. Phys.* **107**, 273 (1997).
- [57] A. Irbäck, C. Peterson, and F. Potthast, *Phys. Rev. E* **55**, 860 (1997).
- [58] S. J. Marrink, H. J. Risselada, S. Yefimov, D. P. Tieleman, and A. H. de Vries, *J. Phys. Chem. B* **111**, 7812 (2007).
- [59] A. L. Rodriguez, C. Vega, and J. J. Freire, *J. Chem. Phys.* **111**, 438 (1999).
- [60] B. A. Berg and T. Neuhaus, *Phys. Lett. B* **267**, 249 (1991); *Phys. Rev. Lett.* **68**, 9 (1992); W. Janke, *Int. J. Mod. Phys. C* **3**, 1137 (1992).
- [61] B. A. Berg, *Fields Institute Communications* **28**, 1 (2000).
- [62] W. Janke, *Physica A* **254**, 164 (1998); and in: *Computer Simulations of Surfaces and Interfaces*, NATO Science Series, II. Mathematics, Physics and Chemistry – Vol. **114**, edited by B. Dünweg, D. P. Landau, and A. I. Milchev (Kluwer, Dordrecht, 2003), pp. 137–157.
- [63] W. Janke and W. Paul, invited review, *Soft Matter* **12**, 642 (2016).
- [64] M. Bachmann, H. Arkin, and W. Janke, *Phys. Rev. E* **71**, 031906 (2005).
- [65] K. Solc and W. H. Stockmayer, *J. Chem. Phys.* **54**, 2756 (1971).
- [66] D. N. Theodorou and U. W. Suter, *Macromolecules* **18**, 1206 (1985).
- [67] V. Blavatska and W. Janke, *J. Chem. Phys.* **133**, 184903 (2010).
- [68] J. Vymětal and J. Vondrášek, *J. Phys. Chem. A* **115**, 11455 (2011).
- [69] V. Blavatska and W. Janke, *J. Chem. Phys.* **136**, 104907 (2012).
- [70] B. Efron, *The Jackknife, the Bootstrap and Other Resampling Plans* (Society for Industrial and Applied Mathematics [SIAM], Philadelphia, 1982).
- [71] W. Janke, *Monte Carlo methods in classical statistical physics*, in: *Computational Many-Particle Physics*, Wilhelm & Else Heraeus Summerschool, Greifswald, edited by H. Fehske, R. Schneider, and A. Weiße, *Lect. Notes Phys.* **739** (Springer, Berlin, 2008), pp. 79–140.
- [72] W. Janke, *Monte Carlo simulations in statistical physics – From basic principles to advanced applications*, in: *Order, Disorder and Criticality: Advanced Problems of Phase Transition Theory*, Vol. 3, edited by Y. Holovatch (World Scientific, Singapore, 2012), pp. 93–166.
- [73] V. Lesins and E. Ruckenstein, *Colloid Polym. Sci.* **266**, 1187 (1988).
- [74] V. Lesins and E. Ruckenstein, *J. Colloid Interface Sci.* **132**, 566 (1989).

# Polymer Adsorption on Curved Surfaces

Handan Arkin<sup>1,2,\*</sup> and Wolfhard Janke<sup>1,†</sup>

<sup>1</sup>*Institut für Theoretische Physik, Universität Leipzig, Postfach 100 920, D-04009 Leipzig, Germany*

<sup>2</sup>*Department of Physics Engineering, Faculty of Engineering,  
Ankara University, Tandogan, 06100 Ankara, Turkey*

The conformational behavior of a coarse-grained finite polymer chain near an attractive spherical surface was investigated by means of multicanonical Monte Carlo computer simulations. In a detailed analysis of canonical equilibrium data over a wide range of sphere radius and temperature, we have constructed entire phase diagrams both for non-grafted and end-grafted polymers. For the identification of the conformational phases, we have calculated several energetic and structural observables such as gyration tensor based shape parameters and their fluctuations by canonical statistical analysis. Despite the simplicity of our model, it qualitatively represents in the considered parameter range real systems that are studied in experiments. The work discussed here could have experimental implications from protein-ligand interactions to designing nano smart materials.

## I. INTRODUCTION

The interaction of macromolecules with differently shaped substrates is particularly important for interdisciplinary research and nano-technological applications including, e.g., the fabrication of biosensors [1] and peptide adhesion [2] to metals [3, 4] or semiconductors [5–7]. Gaining knowledge of structure formation for a variety of interfaces has therefore been a challenging subject of numerous experimental, theoretical and computational investigations. This includes thermodynamic studies of polymers at planar surfaces [8–26], and also under pulling force [27, 28], and at curved surfaces such as nano-tubes, nano-strings and nano-particles [29–34]. Polymer adsorption on flat substrates plays an important role within a wide perspective. Due to the many possible applications, these “hard-soft” hybrid systems have been extensively studied from all aspects. For instance, employing a single-chain mean-field theory for polymers grafted to a flat surface has featured different morphologies for which, by controlling the self-assembly conditions, non-aggregated chains can coexist with micelles [35]. The understanding of the conformational properties of a polymer requires systematic studies because of the cooperative effect of the monomers in response to different system conditions. The structuring effect of an attractive substrate results in a rich phase behavior caused by the competition between monomer-monomer and monomer-surface interaction.

By performing Monte Carlo simulations for detailed atomistic and generic coarse-grained lattice and continuum models, many studies have been done to investigate nano-particle–polymer interactions for different geometries, such as cylinder and sphere [36]. Using computer simulations, Barr and Panagiotopoulos [37] studied a system of polymers grafted to a spherical nano-particle in salt solution to gain insight into the conformational behavior of polymers on curved surfaces. Silver and gold nano-particles have also been considered experimentally as catalyst for enhanced amyloid peptide fibrillation [38–40]. Tanaka *et al.* [41, 42] examined the freezing transition of compact polyampholytes, for both single and multiple chains. There has been a number of studies of these systems to determine the effects of surface charge densities [43] and solvent conditions on the morphologies of polymer chains. Furthermore adsorption of charged chains such as polyelectrolytes by oppositely charged surfaces is also an important aspect in surface and colloidal science [44, 45]. Because of the electrostatic attraction between chains and surfaces, a charged chain tends to be adsorbed onto the surface. These studies are also extended to oppositely charged blocks on the chains [46], and Dobrynin and Rubinstein [47, 48] addressed typical adsorption regimes for a salt-free environment using scaling law arguments. The interaction between polyelectrolytes and small spheres of opposite charge is of interest for many problems such as interaction between polyelectrolytes and micelles or formation of nucleosomal complex between DNA and proteins [49, 50].

Given the plethora of specific applications, it is important to complement such detailed studies with investigations of generic models that focus on the most characteristic parameters of the systems and can hence provide a broad overview of the involved phenomena. In this spirit we have recently investigated the purely steric confinement effect of a spherical cage on a coarse-grained flexible polymer chain to determine the influence on the location of the collapse

---

\*E-mail: Handan.Olgar@eng.ankara.edu.tr

†E-mail: Wolfhard.Janke@itp.uni-leipzig.de;

Homepage: <http://www.physik.uni-leipzig.de/CQT.html>

and freezing transitions [51]. Another hybrid system under consideration was a polymer chain *inside* an attractive spherical cage for which we have constructed the phase diagram depending on the attraction strength of the sphere inner wall and the temperature [52, 53] and investigated the ground-state properties [54]. We have also compared the results with the case of an attractive flat surface [55]. Both systems exhibit a rich phase behavior ranging from highly ordered, compact to extended, random coil structures.

Here, we consider the opposite situation: A nano-sphere whose attractive *outer* spherical surface is the target for the adsorbing polymer. This problem could have practical implications for a broad variety of applications ranging from protein-ligand binding, designing smart sensors to molecular pattern recognition [56–59] and for the discovery of new drugs that bind to specific receptors. Therefore it is interesting to study the adsorption of macromolecules on different types of substrates and identify the conformational changes that a polymer can experience at the interface. In this paper, we are going to investigate a simple coarse-grained polymer model interacting with a spherical surface of varying curvature by means of multicanonical Monte Carlo computer simulations. This method enables us to give an overview of the different structural phases of a flexible polymer chain over a wide range of sphere radius and temperature. In a comparative study, we consider the two cases of non-grafted and end-grafted polymer chains.

The rest of the paper is organized as follows. In Section II the model system is described in detail. Our model is a simple model that enables changing parameters on a broad scale, which allows mapping to different real systems that are considered in experiments. The primary parameters that are scanned to obtain two-dimensional phase diagrams are the radius of the nano-particles and the temperature. We kept the adsorption strength constant in this study (whereas we varied it in another earlier study). Then, in Section III the multicanonical Monte Carlo simulation method is briefly reviewed and the measured observables are introduced, where special attention is paid to invariants of the gyration tensor. Section IV presents and discusses our main results, the phase diagrams for the two systems under consideration. Finally, Section V concludes the paper with a summary of our findings.

## II. MODEL

### A. Bead-stick polymer model

The polymer chain is described by a generic, coarse-grained continuum model for homopolymers which has also been used for studies of heteropolymers in the frame of the hydrophobic-polar model [60, 61]. As in lattice models, the adjacent monomers are connected by rigid covalent bonds. Thus, the distance is kept fixed and set to unity, fixing the length scale. The contact interaction of lattice models is replaced by a distance-dependent 12 – 6 Lennard-Jones (LJ) potential,

$$E_{\text{LJ}} = 4\epsilon_{\text{LJ}} \sum_{i=1}^{N-2} \sum_{j=i+2}^N \left[ \left( \frac{\sigma}{r_{ij}} \right)^{12} - \left( \frac{\sigma}{r_{ij}} \right)^6 \right], \quad (1)$$

accounting for short-range excluded volume repulsion and long-range interaction of non-bonded monomers at distance  $r_{ij} = |\vec{r}_i - \vec{r}_j|$ . Each summand in (1) is minimized for  $r_{ij} = 2^{1/6}\sigma$  where it contributes  $-\epsilon_{\text{LJ}}$  to  $E_{\text{LJ}}$ . In the simulations we set  $\epsilon_{\text{LJ}}$  to unity, fixing the energy scale, and choose  $\sigma = 1$ . This model was first employed in two dimensions [60, 61] and later generalized to three-dimensional AB proteins [62–64], partially with modifications taking implicitly into account additional torsional energy contributions of each bond. For consistency with our previous work [15, 20, 21, 52–55, 64] we kept a very weak bending energy  $E_{\text{bend}} = \varkappa \sum_{i=1}^{N-2} (1 - \cos \vartheta_i)$  with  $\varkappa = 1/4$  and  $\vartheta_i$  denoting the angle between adjacent bonds ( $\cos \vartheta_i = (\vec{r}_{i+1} - \vec{r}_i) \cdot (\vec{r}_{i+2} - \vec{r}_{i+1})$ ). For such a small bending stiffness, however, the statistical properties are hardly distinguishable from a truly flexible ( $\varkappa = 0$ ) polymer (see, e.g., Fig. 1 in Ref. [65]).

### B. Surface Interaction

In this work, we assume that the polymer chain interacts with an attractive spherical surface. As in our previous work [52–55] the interaction of the polymer chain monomers and the attractive sphere is modeled by the surface energy  $E_s = \sum_{i=1}^N V_s(r_i)$  where

$$V_s(r_i) = 4\pi\epsilon_s \frac{R_s}{r_i} \left\{ \frac{1}{5} \left[ \left( \frac{\sigma_s}{r_i - R_s} \right)^{10} - \left( \frac{\sigma_s}{r_i + R_s} \right)^{10} \right] - \frac{\epsilon}{2} \left[ \left( \frac{\sigma_s}{r_i - R_s} \right)^4 - \left( \frac{\sigma_s}{r_i + R_s} \right)^4 \right] \right\}. \quad (2)$$

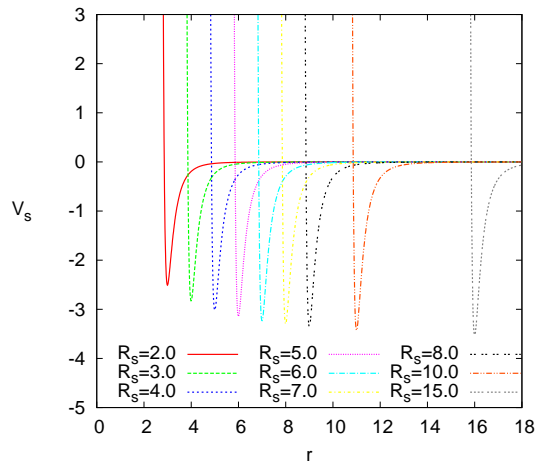


FIG. 1: The functional dependence of the attractive sphere potential (2) (with  $\epsilon_s = \sigma_s = \epsilon = 1$ ) for different values of the sphere radius  $R_s$ .

Here  $R_s$  is the radius of the sphere,  $r_i = (x_i^2 + y_i^2 + z_i^2)^{1/2} \geq R_s$  is the distance of a monomer to the origin and  $x_i, y_i, z_i$  are the coordinates of monomers, and  $\sigma_s, \epsilon_s$ , and  $\epsilon$  are set to unity. The functional dependence of the potential  $V_s(r_i)$  is shown in Fig. 1 for selected  $R_s$  values which are used in the simulations. For sufficiently large spheres and  $r_i$  close to the surface,  $r_i \approx R_s$ , we can neglect the terms  $(\sigma/2R_s)^{10}$  and  $(\sigma/2R_s)^4$  and approximate [55]

$$V_s(r_i) \approx 4\pi\epsilon_s \left[ \frac{1}{5} \left( \frac{\sigma}{r_i - R_s} \right)^{10} - \frac{\epsilon}{2} \left( \frac{\sigma}{r_i - R_s} \right)^4 \right], \quad (3)$$

which is a standard 10 – 4 Lennard-Jones potential with  $V_s^{\min} = -4\pi\epsilon_s(3/10)\epsilon^{5/3}R_s/(R_s + \sigma_s\epsilon^{-1/6})$  at  $r_i^{\min} = R_s + \sigma_s\epsilon^{-1/6}$ .

The total energy  $E = E_{\text{LJ}} + E_{\text{bend}} + E_s$  governs the statistical properties at temperature  $T$  respectively thermal energy  $k_B T$ , where  $k_B$  is the Boltzmann constant. In the following we set  $k_B$  to unity, fixing the temperature scale. The most interesting phenomena result from the competition of intrinsic monomer-monomer and monomer-surface wall interactions. For instance in the case of adsorption of polyelectrolyte chains onto oppositely charged interfaces, the electrostatic potential controls the competition of polymer-surface adsorption-desorption behavior.

Our primary goal of this study is to obtain a broad overview of the phase diagram in the  $R_s - T$  plane. To make contact to specific experimental polymer-substrate systems one may identify the empirical (dimensionful) coupling parameters of, say, the Martini force field [66] with the (dimensionless) parameters of our coarse-grained model. For instance, from Table 1 in Ref. [67] we read off that methylene has  $\epsilon_{\text{phys}} = 104 \times 8.31/1000 = 0.86\text{kJ/mol}$  which approximately corresponds to  $\epsilon_{\text{LJ}} = 1.0$  in our model. It follows that the 20mer (4 methylenes per bead) considered in our study corresponds approximately to n-C80. Similarly, the substrate maps approximately onto a polystyrene colloidal sphere, but its adsorption propensity is weaker than that of carbon or silica.

### III. SIMULATION SETUP

#### A. Multicanonical method

In order to obtain statistical results of sufficient accuracy we applied the multicanonical (muca) Monte Carlo algorithm [68–70] (for reviews, see Refs. [71–73]), where the energy distribution is flattened artificially allowing, in principle, for a random walk of successive states in energy space. This flattening is controllable and therefore reproducible. To this end, the Boltzmann probability is multiplied by a weight factor  $W(E)$ , which in our case is a function of the total energy  $E = E_{\text{LJ}} + E_{\text{bend}} + E_s$ . Then the multicanonical probability for a state or conformation  $\{\mathbf{x}\}$  with energy  $E(\{\mathbf{x}\})$  reads  $p_{\text{muca}}(E) = \exp(-E/k_B T)W(E)$ , up to an unimportant multiplicative factor. In order to obtain a multicanonical or “flat” distribution, the initially unknown weight function  $W(E)$  has to be determined iteratively: In the beginning, the weights  $W^{(0)}(E)$  are set to unity for all energies letting the first run be a usual Metropolis simulation which yields an estimate  $H^{(0)}(E)$  for the canonical distribution. This histogram is used to

determine the next guess for the weights, the simplest update is to calculate  $W^{(1)}(E) = W^{(0)}(E)/H^{(0)}(E)$ . Then the next run is performed with probabilities  $p_{\text{muca}}^{(1)}(E) = \exp(-E/k_B T)W^{(1)}(E)$  of states with energy  $E$ , yielding  $H^{(1)}(E)$  and  $W^{(2)}(E) = W^{(1)}(E)/H^{(1)}(E)$ , and so on. The iterative procedure is continued until the weights are appropriate in a way that the multicanonical histogram  $H(E)$  is “flat”. After having determined accurate weights  $W(E)$ , they are kept fixed and following some thermalization sweeps a long production run is performed, where statistical quantities  $O$  are obtained multicanonically,  $\langle O \rangle_{\text{muca}} = \sum_{\{\mathbf{x}\}} p_{\text{muca}}(E(\{\mathbf{x}\}))O(\{\mathbf{x}\})/Z_{\text{muca}}$  with the multicanonical partition function  $Z_{\text{muca}} = \sum_{\{\mathbf{x}\}} p_{\text{muca}}(E(\{\mathbf{x}\}))$ . The canonical statistics is obtained by reweighting the multicanonical to the canonical distribution, i.e., canonical expectation values are computed as  $\langle O \rangle = \langle OW^{-1} \rangle_{\text{muca}}/\langle W^{-1} \rangle_{\text{muca}}$ . For a recent review of these methodological aspects in the context of polymer simulations, see Refs. [74, 75].

## B. Observables

To obtain as much information as possible about the canonical equilibrium behavior, we define the following suitable quantities  $O$ . Next to the canonical expectation values  $\langle O \rangle$ , we also determine the fluctuations about these averages, as represented by the temperature derivative  $d\langle O \rangle/dT = (\langle OE \rangle - \langle O \rangle \langle E \rangle)/T^2$ . We use generic units, in which  $k_B = 1$ .

In order to identify conformational transitions, the specific heat (per monomer)  $C_V(T) = (\langle E^2 \rangle - \langle E \rangle^2)/NT^2$  with  $\langle E^k \rangle = \sum_E g(E)E^k \exp(-E/T)/\sum_E g(E) \exp(-E/T)$  is calculated from the density of states  $g(E)$ . The density of states was found (up to an unimportant overall normalization constant) by reweighting the multicanonical energy distribution obtained with multicanonical sampling to the canonical distribution. Details are given in Ref. [64].

Apart from the specific heat, several structural quantities are of interest. In order to check the structural compactness of conformations or to identify the possible dispersion of conformations because of adsorption, the radius of gyration of the conformations is calculated. The radius of gyration is a measure for the extension of the polymer and defined by  $R_g^2 \equiv \sum_{i=1}^N (\vec{r}_i - \vec{r}_{\text{cm}})^2/N = \sum_{i=1}^N \sum_{j=1}^N (\vec{r}_i - \vec{r}_j)^2/2N^2$  with  $\vec{r}_{\text{cm}} = \sum_{i=1}^N \vec{r}_i/N$  being the center-of-mass of the polymer.

We also calculated various shape descriptors derived from the gyration tensor [76–79] which is defined as

$$S = \frac{1}{N} \begin{pmatrix} \sum_i (x_i - x_{\text{cm}})^2 & \sum_i (x_i - x_{\text{cm}})(y_i - y_{\text{cm}}) & \sum_i (x_i - x_{\text{cm}})(z_i - z_{\text{cm}}) \\ \sum_i (x_i - x_{\text{cm}})(y_i - y_{\text{cm}}) & \sum_i (y_i - y_{\text{cm}})^2 & \sum_i (y_i - y_{\text{cm}})(z_i - z_{\text{cm}}) \\ \sum_i (x_i - x_{\text{cm}})(z_i - z_{\text{cm}}) & \sum_i (y_i - y_{\text{cm}})(z_i - z_{\text{cm}}) & \sum_i (z_i - z_{\text{cm}})^2 \end{pmatrix}. \quad (4)$$

Transformation to the principal axis system diagonalizes  $S$ ,

$$S = \text{diag}(\lambda_1, \lambda_2, \lambda_3), \quad (5)$$

where we assume that the eigenvalues of  $S$  are sorted in descending order, i.e.,  $\lambda_1 \geq \lambda_2 \geq \lambda_3$ . The first invariant of  $S$  gives the squared radius of gyration,

$$\text{Tr} S = \lambda_1 + \lambda_2 + \lambda_3 = R_g^2, \quad (6)$$

which agrees with the definition given above. The second invariant shape descriptor, or relative shape anisotropy, is defined as

$$\kappa^2 \equiv A_3 = \frac{3}{2} \frac{\text{Tr} \hat{S}^2}{(\text{Tr} S)^2} = 1 - 3 \frac{\lambda_1 \lambda_2 + \lambda_2 \lambda_3 + \lambda_3 \lambda_1}{(\lambda_1 + \lambda_2 + \lambda_3)^2}, \quad (7)$$

where  $\hat{S} = S - \frac{1}{3}(\text{Tr} S)I$  with unit tensor  $I$ . It reflects both the symmetry and dimensionality of a polymer conformation. This parameter is limited between the values of 0 and 1. It reaches 1 for an ideal linear chain and drops to zero for highly symmetric conformations. For planar symmetric objects, the relative shape anisotropy converges to the value of 1/4 [76–80].

The distance of the center-of-mass,  $r_{\text{cm}}$ , of the polymer to the surface also provides clear evidence that the polymer is freely moving or that it is very close to the surface and just adsorbed. Another useful quantity is the mean number of monomers  $\langle N_s \rangle$  docked to the surface, which plays the role of an order parameter for the adsorption transition. A single-layer structure is formed if all monomers are attached to the sphere; if none is attached, the polymer is desorbed. The sphere potential is a continuous potential, and in order to distinguish monomers docked to the sphere from those not being docked, it is reasonable to introduce a cutoff. We define a monomer  $i$  as being “docked” if  $r_i - R_s < r_c \equiv 1.2$ . The corresponding measured quantity is the average number  $\langle N_s \rangle$  of monomers docked to the surface. This can be expressed as  $N_s = \sum_{i=1}^N \Theta(r_c - r_i)$ , where  $\Theta(r)$  is the Heaviside step function.



FIG. 2: (Color online) Start configurations of the simulations: (a) non-grafted and (b) end-grafted polymers of length  $N = 20$ .

### C. Computational details

In our simulations, the polymer chain length is  $N = 20$  and we set  $\epsilon = 1.0$  in the surface potential (2) large enough to allow adsorption of the polymer to the sphere surface. We consider two different situations, one is the case where the polymer is allowed to move freely in the space around the sphere over a distance  $L = 60 - R_s$  from its surface (i.e., the nano-sphere of radius  $R_s$  is centered in a spherical container of radius 60 with a purely steric wall), which is called the “free” or “non-grafted” case, and in the second case it is grafted with one end to the surface (“end-grafted”).

We have done simulations with different sizes of the sphere. The random initial configurations for the non-grafted and end-grafted cases of the simulation are sketched in Figs. 2(a) and (b). The total energy of the system is composed of the pure polymer chain energy  $E_{LJ} + E_{\text{bend}}$  and the polymer chain attractive sphere interaction energy  $E_s$ . The initial configuration of the polymer chain is randomly generated. For the determination of the multicanonical weights we performed 200 iterations with at least  $10^5$  sweeps each. In the production period,  $10^8$  sweeps were generated to have reasonable statistics for estimating the thermodynamic quantities. Statistical errors are estimated with the standard Jackknife technique [81–83].

## IV. RESULTS

### A. Phase diagrams

To give an overview at the beginning, we start by presenting in Fig. 3 the main result of our study: The phase structure for (a) non-grafted and (b) end-grafted polymers derived from all of our observables as summarized by phase diagrams in the  $R_s - T$  plane. These phase diagrams are constructed by combining all the informations coming from the canonical expectation values of our observables and their temperature derivatives described in more detail in the next two subsections. Some of our observables exhibit a peak at all of the transitions in the phase diagram, while others are only sensitive to one of them. For example, the collapse transition line at  $T \approx 0.8$  is seen quite clearly from the peak in the temperature derivative of the canonical expectation value of the radius of gyration (6) and as a small shoulder in the invariant shape anisotropy (7). Naturally, this is further complemented by information coming directly from the eigenvalues of the gyration tensor. On the other hand, the adsorption line running roughly between  $T \approx 1.5$  (small  $R_s$ ) and  $T \approx 2.5$  (large  $R_s$ ) is most clearly constructed by looking at the mean distance of the center-of-mass of the polymer to the surface and the mean number of monomers adsorbed onto the surface, which plays the role of an order parameter for this transition. Since we are dealing with a finite system, it is not possible to determine the transition lines precisely: The transition lines still vary with chain length  $N$  and the observables have broad peaks. Thus we have a certain band width which approximately covers the different peaks in the observables (and strictly speaking one should talk of “pseudo-transitions” instead of “transitions” and “pseudo-phases” instead of “phases”, but for brevity we will suppress the attribute “pseudo” in the following).

In the phase diagrams the radius of the sphere increases from left to right and the temperature increases from bottom

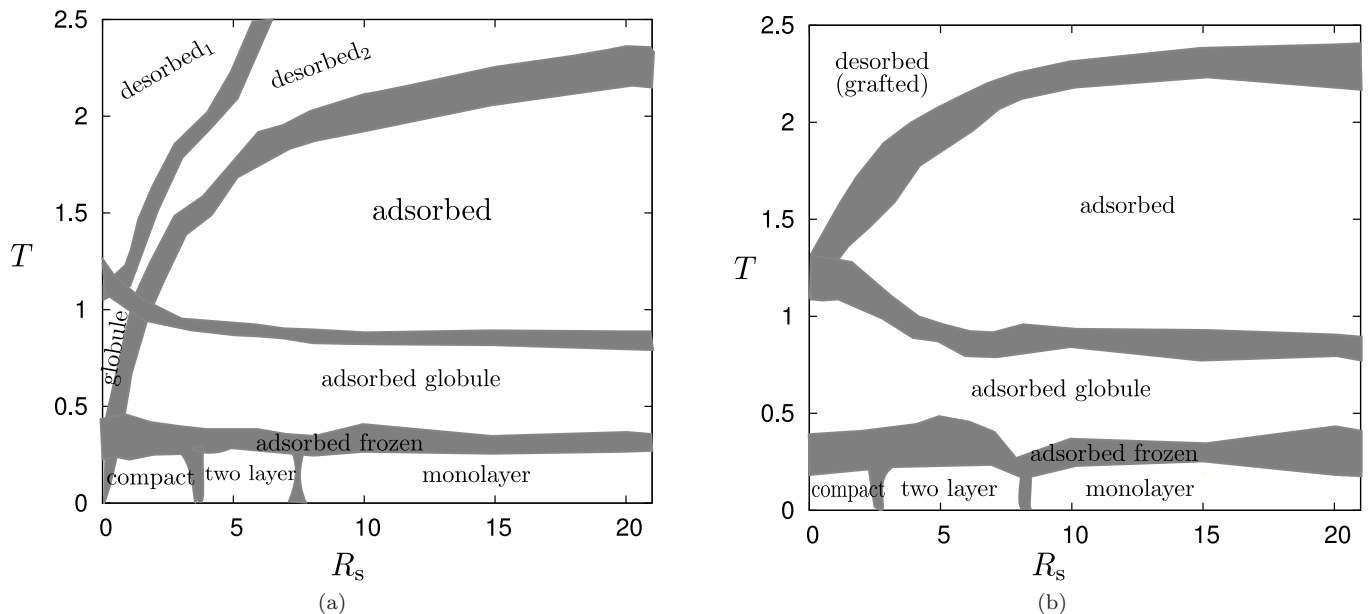


FIG. 3: The phase diagram of the homopolymer-attractive spherical surface system for (a) a non-grafted and (b) an end-grafted polymer as obtained from extensive multicanonical simulations. The grey bands separate the individual conformational phases. The band width shows the variation of the peaks of temperature derivatives of different energetic and structural observables which have been analyzed simultaneously. In our simulations, the polymer chain length is  $N = 20$  and we set  $\epsilon = 1.0$  for the surface attraction strength.

to top. The grey bands separate the individual conformational phases. For high temperature, the polymer behaves in both cases similarly to a free polymer where the typical conformations are desorbed and extended random coils. In the non-grafted case with small sphere radius  $R_s$ , decreasing the temperature causes the (three-dimensional) collapse transition into globular conformations which are still in the desorbed phase. But below the freezing transition all the compact conformations are adsorbed. In contrast, for the end-grafted case all conformations are already adsorbed below the collapse transition. There is no desorbed globule phase in the grafted phase diagram. One more difference occurred also in the high-temperature desorbed phase. In the non-grafted case some structural observables give indication for some changes in the desorbed phase. When we carefully analyze the conformations we see that those in the “desorbed<sub>1</sub>” phase are far away from the sphere surface while the conformations in the “desorbed<sub>2</sub>” phase are almost adsorbed. Thus they feel very strongly the surface effect. Because of the grafting, this is not the case for an end-grafted polymer. Increasing the sphere radius approximately to  $R_s \approx 7.0$  leads to a very fast increase in the adsorption transition temperature, but after this value it increases slowly. The adsorption transition separates the regions of desorbed and adsorbed phases. Besides the collapse, adsorption, and freezing transitions, the most pronounced transition is the layering transition which occurs for low temperatures at  $R_s \approx 7.0$  and separates the region of planar conformations which are monolayers of totally adsorbed conformations from the two-layer conformations. Another low-temperature transition is coming into play at  $R_s \approx 3.0$ , where two-layer conformations change to compact conformations (which look almost like a sphere).

The representative conformations that predominate in the different structural phases are depicted in Fig. 4 for the case of a non-grafted polymer. The observed structural phases for this case can be briefly summarized as follows:

**Desorbed<sub>1</sub>:** Random coil structures with no surface contacts. These conformations freely circulate in the simulation space and are far away from the surface of the sphere [Fig. 4(a)].

**Desorbed<sub>2</sub>:** Desorbed conformations, but they are almost adsorbed. The conformations feel the influence of the surface [Fig. 4(b)].

**Adsorbed:** Partially adsorbed, extended conformations [Fig. 4(c)].

**Adsorbed Globule:** Partially adsorbed conformations [Fig. 4(d)].

**Globule:** Desorbed globule conformations. These conformations are only seen in the non-grafted phase diagram [Fig. 4(e)].

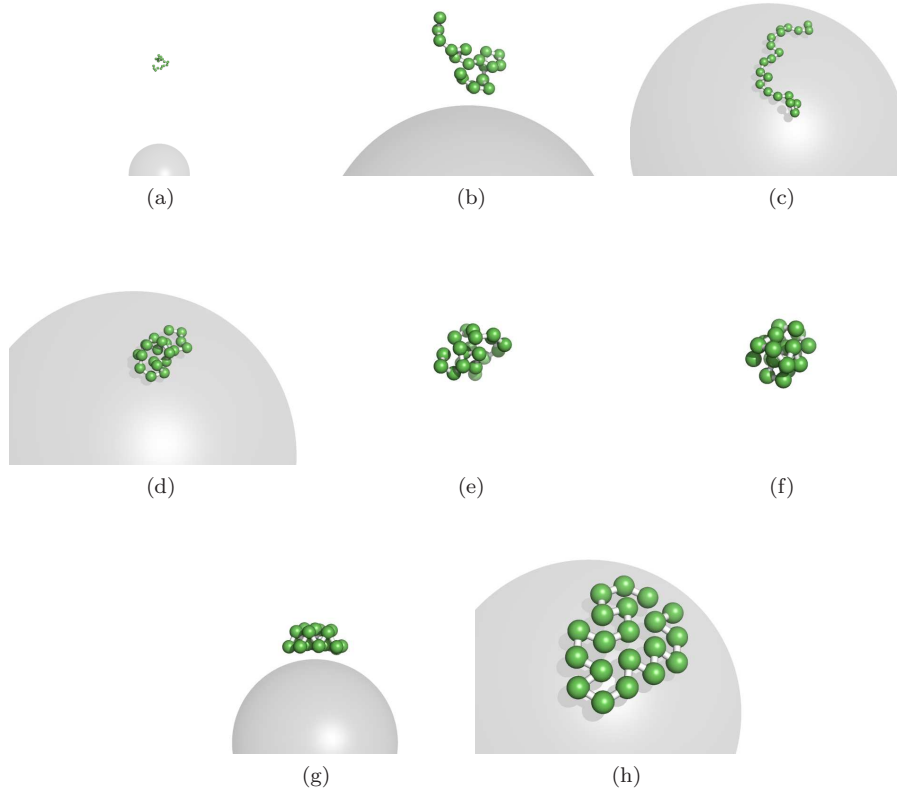


FIG. 4: (Color online) Typical conformations for the regions (a) desorbed<sub>1</sub>, (b) desorbed<sub>2</sub>, (c) adsorbed, (d) adsorbed globule, (e) globule, (f) compact, (g) two layer, and (h) monolayer in the phase diagram for a non-grafted polymer.

**Compact:** Partially adsorbed, globular conformations like a drop on the wall of the sphere [Fig. 4(f)].

**Two Layer:** Partially adsorbed, compact conformations. These are two-layer structures. The lower layer of the conformations is adsorbed and lies on the wall of the sphere [Fig. 4(g)].

**Monolayer:** Completely adsorbed, compact conformations. These single-layer structures lie on the surface of the sphere and fit the sphere wall perfectly [Fig. 4(h)].

In the following two sections we will discuss in more detail how these phase diagrams have been obtained by analyzing energetic and structural observables.

## B. Energetic fluctuations

Figure 5 displays the specific-heat curves  $C_V(T)$  as a function of temperature  $T$  for different values of sphere radius  $R_s$  for (a) the non-grafted and (b) the end-grafted case. In both cases the specific heat signals two transitions: one is the low-temperature transition which is almost at the same temperature ( $T \approx 0.3$ ) for all different  $R_s$  values. This is the freezing transition which does not differ much for non-grafted and end-grafted chains. The second transition is quite pronounced in the non-grafted case but exhibits only a weak signal (a shoulder at  $T \approx 2.0$ ) for the grafted polymer. This is the adsorption transition, which separates desorbed and adsorbed conformations. It comes into play at higher temperatures than the freezing transition and depends quite strongly on the sphere radius. This is consistent with previous observations that for non-grafted polymers of finite length this transition has a first-order-like signature (which eventually crosses over to second-order-like in the infinite chain-length limit) [21, 50, 84], whereas for grafted polymers it always looks like a continuous transition. In both cases, increasing the sphere radius causes an increase in the adsorption transition temperature.

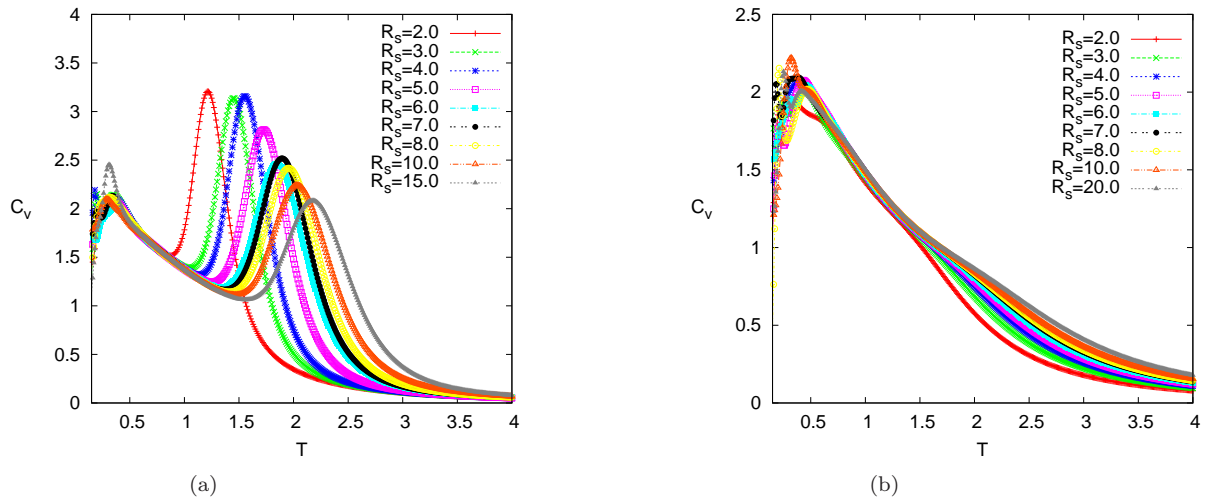


FIG. 5: (Color online) Specific heat as a function of temperature for different sphere radii  $R_s$  for the (a) non-grafted and (b) end-grafted case (polymer length  $N = 20$ , surface attraction strength  $\epsilon = 1.0$ ).

### C. Structural parameters and fluctuations

#### 1. Radius of gyration $R_g$

The radius of gyration  $\langle R_g \rangle$  (the first invariant of the gyration tensor) and its temperature derivative  $d\langle R_g \rangle/dT$  are shown in Fig. 6 as a function of temperature for both the non-grafted and end-grafted cases, respectively. For small values of the sphere radius  $R_s = 0.5, 1.0$ , the most compact conformations occur in the low-temperature region with an average  $\langle R_g \rangle \approx 1.23$  (data not shown). Slightly increasing the  $R_s$  value causes an increase in the average  $\langle R_g \rangle$  value to about 1.4. Increasing the  $R_s$  parameter further, the curve for  $R_s = 7.0$  of Fig. 6(a) in the non-grafted case has a minimum behavior at low temperatures. As a function of temperature the radius of gyration is monotonically increasing for all  $R_s$  values except beyond  $R_s = 7.0$ , where the layering transition occurs. Supporting information is also gained from the relative shape anisotropy parameter in Fig. 7. If we now look at the temperature derivative of the radius of gyration in Fig. 6(c), we detect three maxima for each  $R_s$  curve. The first peak at low temperatures ( $T \approx 0.3$ ) indicates the freezing transition quite clearly, the second peak around  $T \approx 0.8$  can be identified with the (two-dimensional) collapse transition, and the third, strongly moving peak in the region  $T \approx 1.5 - 3.0$  signals the adsorption transition. For the end-grafted case these signals are generally weaker. In Fig. 6(d), the first two maxima are still discernable, but the adsorption transition is hardly reflected.

#### 2. Invariant shape anisotropy parameter $\kappa^2$

Also the relative shape anisotropy parameter  $\langle \kappa^2 \rangle$  (the second invariant of the gyration tensor) presented in Fig. 7 gives rich information and supports our findings derived from  $\langle R_g \rangle$ . As discussed above, in the non-grafted case, the desorbed phase is divided into two regions which are called “desorbed<sub>1</sub>” and “desorbed<sub>2</sub>”. The boundary between these two regions is emerging in the temperature derivative  $d\langle \kappa^2 \rangle/dT$  displayed in Fig. 7(c) (and also in  $d\langle R_g \rangle/dT$ ) as a second peak at high temperatures, since the peaks are going to become invisible with increasing  $R_s$  values and also are smaller than the peaks at low temperatures. We have investigated the conformations in both regions in detail and concluded that the conformations in the “desorbed<sub>1</sub>” phase are far away from the surface. On the other hand, the conformations in the “desorbed<sub>2</sub>” phase are almost adsorbed to the sphere boundary, which indicates the influence of the surface on the desorbed phase. Additionally, the relative shape anisotropy parameter  $\langle \kappa^2 \rangle$  clearly gives the phase boundaries at very low temperatures (below the freezing transition at  $T \approx 0.3$ ). The curves in Fig. 7(a) belonging to different  $R_s$  values are grouped at very low temperatures into different  $\kappa^2$  values, indicating the boundaries from compact to two-layer phase, and from two-layer to monolayer phase in the phase diagrams.

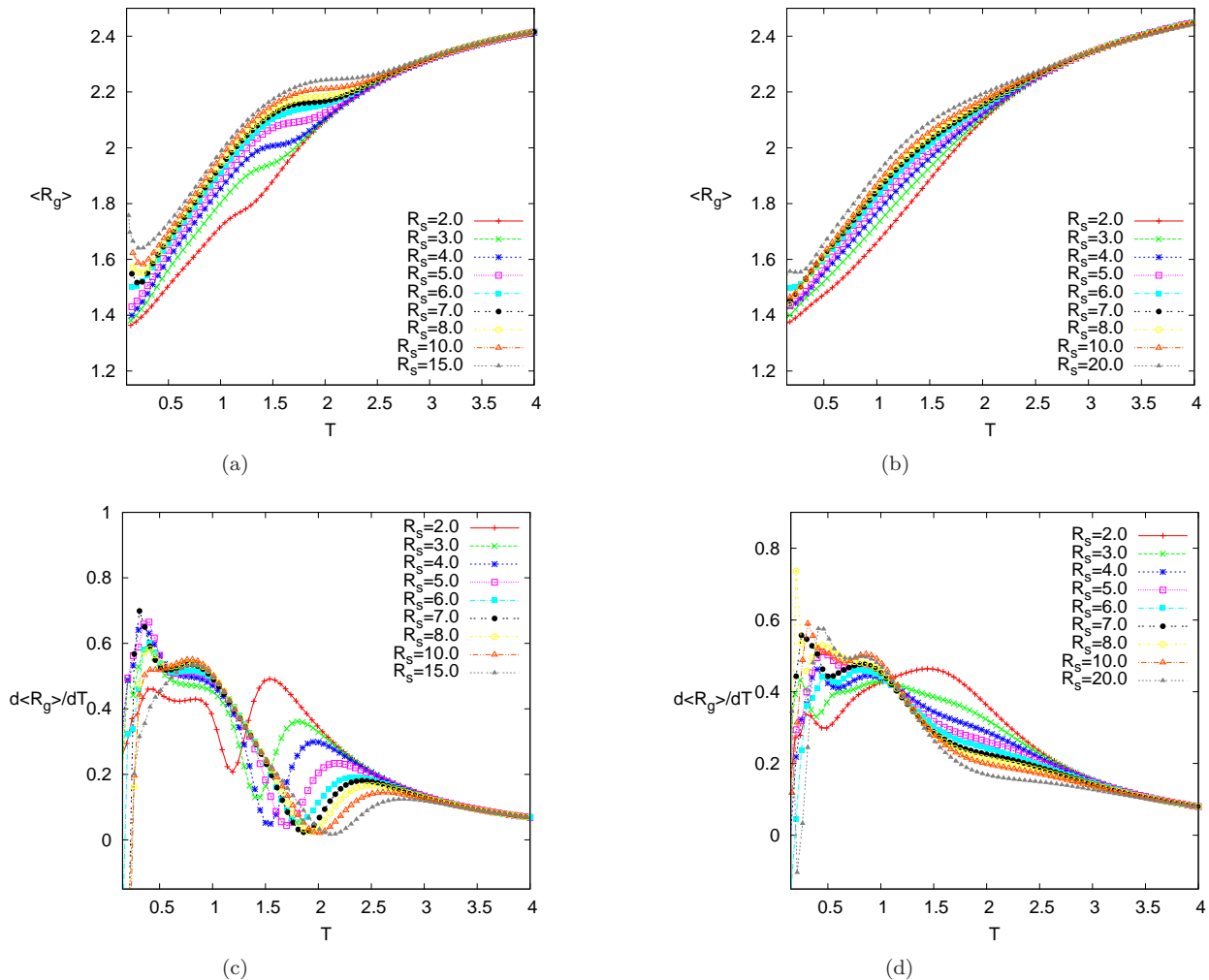


FIG. 6: (Color online) The canonical expectation value of the radius of gyration  $\langle R_g \rangle$  for the (a) non-grafted and (b) end-grafted case, and (c), (d) the corresponding temperature derivatives, for different sphere radii  $R_s$  (polymer length  $N = 20$ , surface attraction strength  $\epsilon = 1.0$ ).

### 3. Center-of-mass distance $r_{cm}$ and number of adsorbed monomers $N_s$

The adsorption transition can be best detected by the distance of the center-of-mass of the polymer to the substrate  $r_{cm} - R_s$  and by the number of adsorbed monomers  $N_s$ , where a monomer is defined to be adsorbed onto the surface if  $r_i - R_s < 1.2$ . The behavior of these two observables, in particular the peaks in their temperature derivative, build the adsorption line in the phase diagrams. Figures 8(a) and (b) give the distance of the center-of-mass of the polymer to the sphere surface for the non-grafted and end-grafted cases, respectively. As can be seen in Fig. 8(a), for high temperatures the non-grafted polymer can move freely within the simulation space and the influence of the surface is minimal for large  $R_s$  values, whereas for small  $R_s$  the influence is mainly steric. Thus, the average center-of-mass distance of the polymer above the surface is nearly half of the simulation space. In contrast, at low temperatures the polymer favors surface contacts and the average center-of-mass distance converges to the minimum location of the potential (cf. Fig. 1). One can clearly detect a quite pronounced peak in its temperature derivative [see Supplementary Material] that divides the phase space into adsorbed and desorbed phases. Consistently with our discussion above, the pronounced tendency of the polymer to make surface contacts can also be identified from the mean number of adsorbed monomers to the surface  $\langle N_s \rangle$  shown in Fig. 9 and the (negative) minima in its temperature derivative [see Supplementary Material]. They are in good agreement with the sharp peaks in the temperature derivative of the distance of the center-of-mass of the polymer which together draw the adsorption line in the phase diagram. By comparing the end-grafted with the non-grafted case, the main difference is found at the adsorption transition:

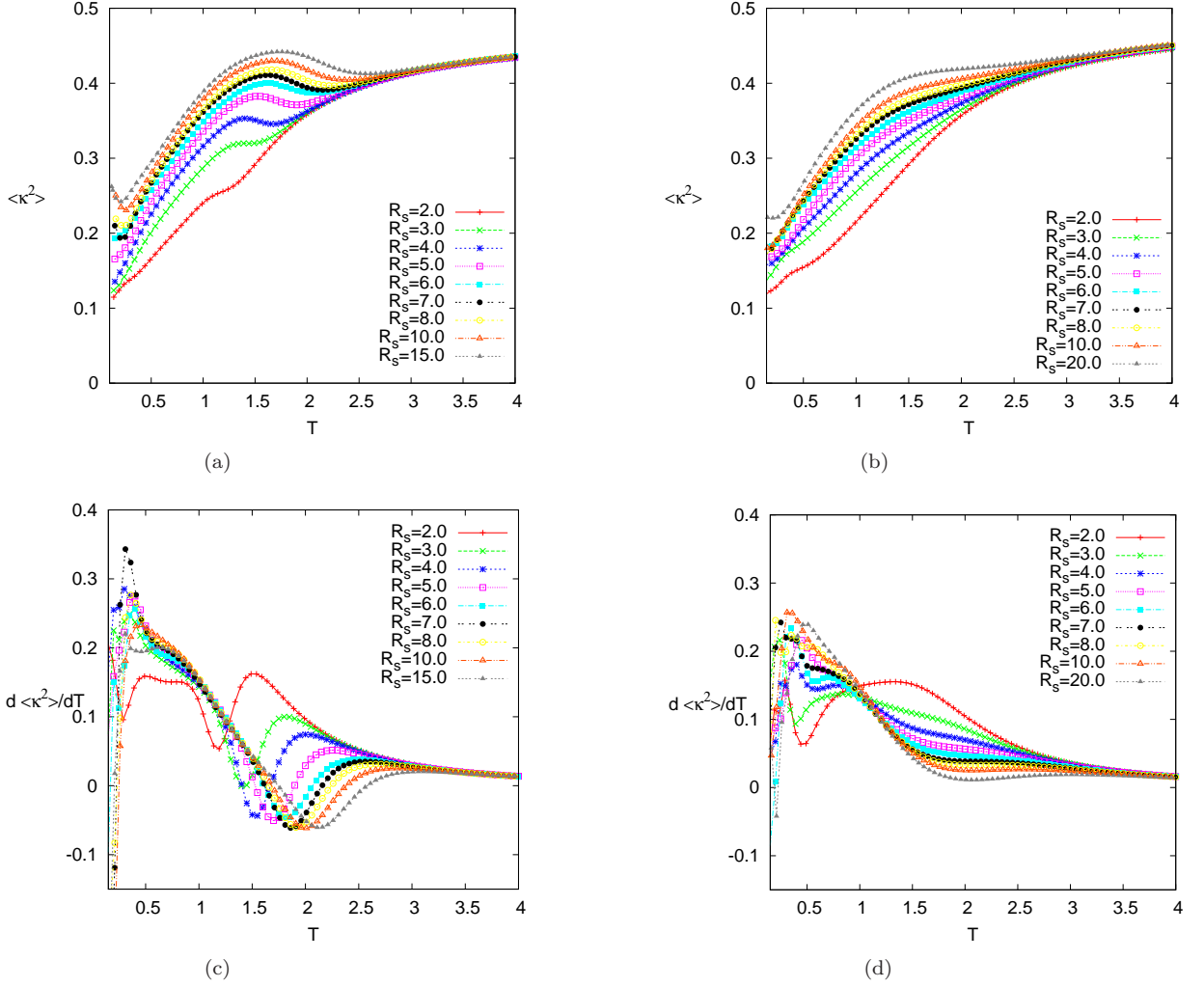


FIG. 7: (Color online) The canonical expectation value of the relative shape anisotropy parameter  $\langle \kappa^2 \rangle$  for the (a) non-grafted and (b) end-grafted case, and (c), (d) the corresponding temperature derivatives, for different sphere radii  $R_s$  (polymer length  $N = 20$ , surface attraction strength  $\epsilon = 1.0$ ).

A crossover occurs from low temperature, where the polymer is adsorbed and the conformations of an end-grafted and a non-grafted polymer are very similar, to high temperatures, where the non-grafted polymer approaches the behavior of a polymer in bulk solution while that of an end-grafted polymer is always affected by the attractive sphere surface. Because of this effect, the adsorption transition for the end-grafted chain is much smoother which can be clearly seen in the  $\langle r_{cm} \rangle$  and  $\langle N_s \rangle$  parameters in Figs. 8(b) and 9(b). In contrast, the adsorption of a non-grafted chain exhibits a first-order-like signature which is also clear from the same structural parameters. Because in the non-grafted case these quantities change sharply as soon as the polymer desorbs, it leaves the influence of the surface field. An end-grafted polymer, on the other hand, cannot leave the surface field.

#### 4. Eigenvalues of the gyration tensor

Finally, the eigenvalues of the gyration tensor which measure the extensions in the principle axis system are extracted to complement the picture. In Figs. 10(a)-(c) they are displayed for different values of  $R_s$  for the non-grafted case. For high temperatures they are in good agreement with the results in our previous study [53], showing the same limit values of the three eigenvalues for random-coil structures, and overall they all support our earlier findings described above. For low temperatures, the curves in Figs. 10(a)-(c) belonging to different  $R_s$  values are also grouped into different  $\langle \lambda_1 \rangle$ ,  $\langle \lambda_2 \rangle$  and  $\langle \lambda_3 \rangle$  values, indicating the boundaries (grey bands) in the phase diagrams which are detected

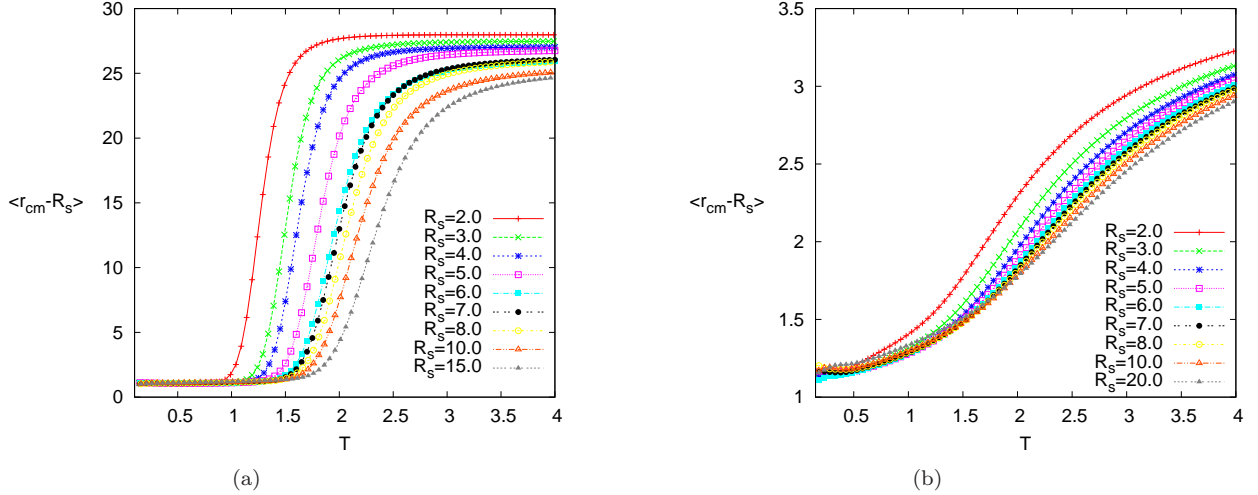


FIG. 8: (Color online) The canonical expectation value of the distance of the center-of-mass of the polymer  $\langle r_{\text{cm}} \rangle$  from the sphere surface for the (a) non-grafted and (b) end-grafted case (polymer length  $N = 20$ , surface attraction strength  $\epsilon = 1.0$ ).

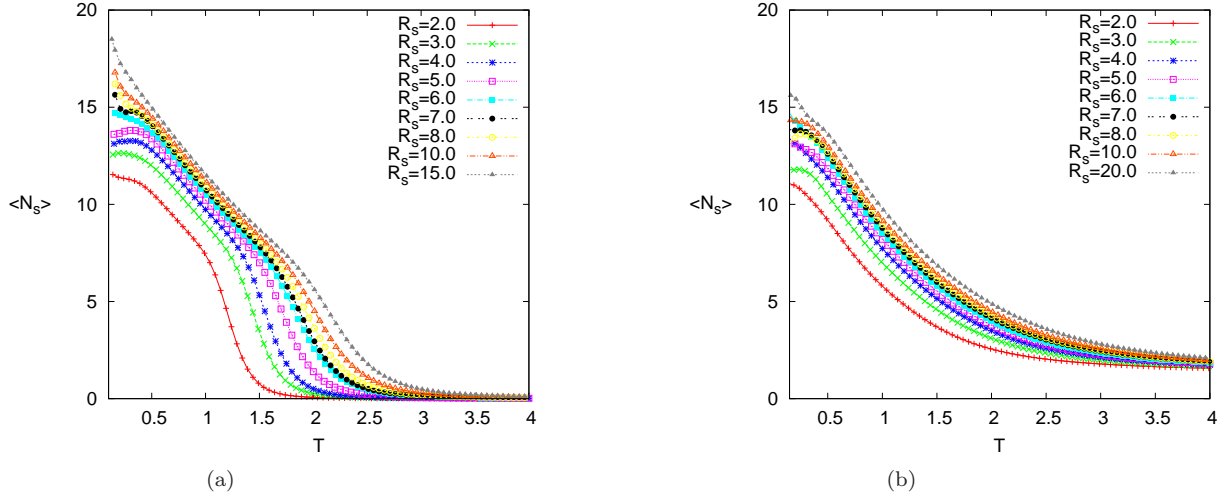


FIG. 9: (Color online) The canonical expectation value of the mean number of docked monomers  $\langle N_s \rangle$  for the (a) non-grafted and (b) end-grafted case (polymer length  $N = 20$ , surface attraction strength  $\epsilon = 1.0$ ).

from the other structural quantities. The most important result deducible from the eigenvalues is that: The third eigenvalue of the gyration tensor  $\langle \lambda_3 \rangle$  converges to small values which means that the extension in the third direction vanishes and the conformations are two-dimensional objects signaling the layering transition. To highlight this finding we show in Fig. 10(d) the ratio of the largest to the smallest eigenvalue  $\langle \lambda_1 / \lambda_3 \rangle$ . For low temperatures below  $T \approx 0.3$ , this ratio assumes relatively small values until  $R_s \approx 6.0$ . Above  $R_s \approx 7.0$  the ratio of the eigenvalues jumps to very much larger values, confirming that the layering transition occurs at this  $R_s$  value, which separates the conformational space from planar conformations. This signal is also reflected in the corresponding temperature derivatives which are compiled in the Supplementary Material.

## V. CONCLUSION

In this paper, we have reported results from extensive multicanonical Monte Carlo computer simulations for investigating the full conformational behavior of a generic coarse-grained finite polymer chain near an attractive spherical surface. In a systematic analysis, over a wide range of sphere radius  $R_s$  and temperature  $T$ , we have constructed the entire phase diagrams for both non-grafted and end-grafted polymers. For the identification of the conformational

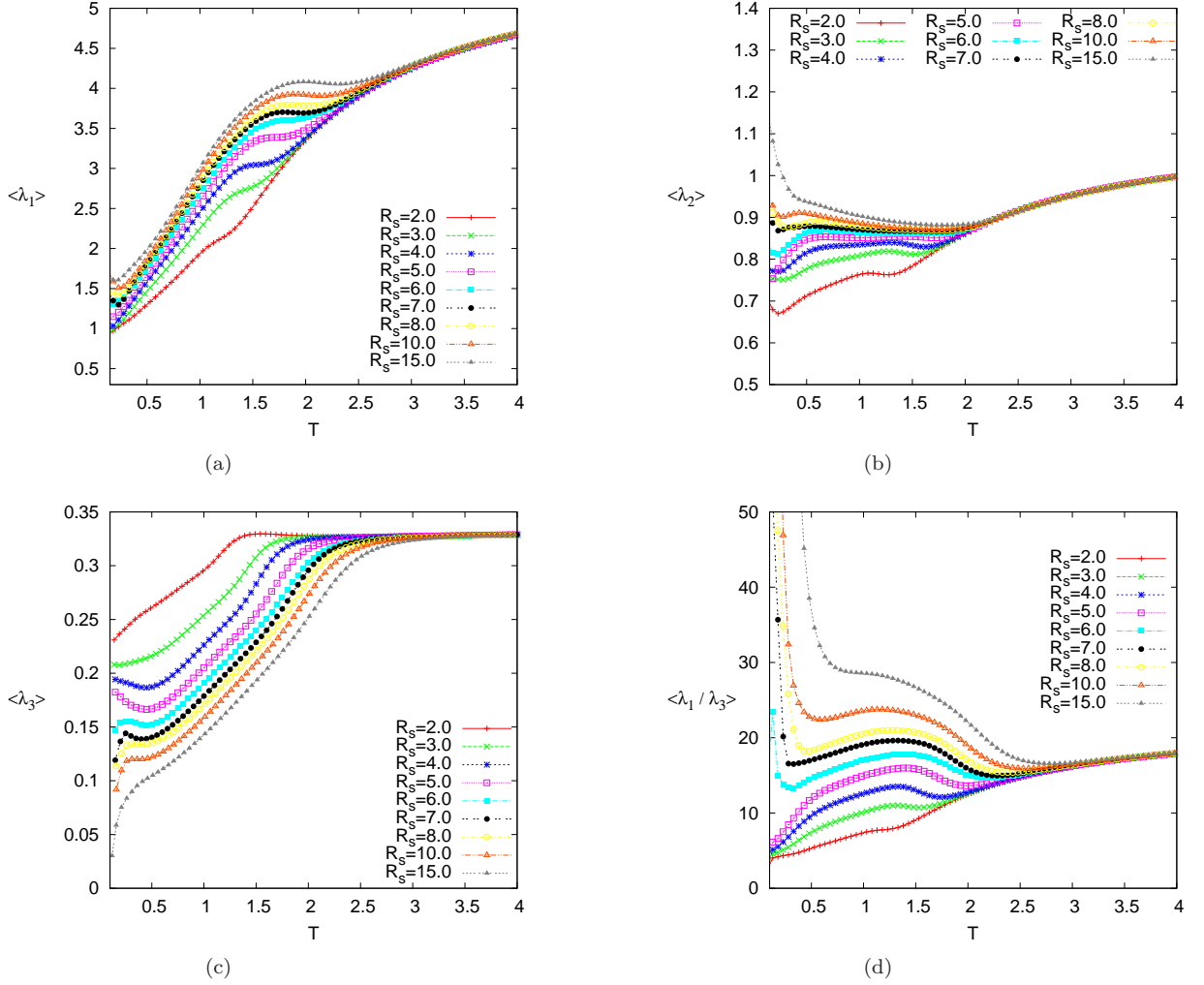


FIG. 10: (Color online) The canonical expectation values of the three eigenvalues  $\langle \lambda_1 \rangle$ ,  $\langle \lambda_2 \rangle$ , and  $\langle \lambda_3 \rangle$  of the gyration tensor and the ratio of the largest to the smallest eigenvalue  $\langle \lambda_1 / \lambda_3 \rangle$  for a non-grafted polymer in the presence of an attractive sphere with different radii  $R_s$  (polymer length  $N = 20$ , surface attraction strength  $\epsilon = 1.0$ ).

phases, we have examined several energetic and structural observables and their fluctuations by canonical statistical analysis. The transition lines in the phase diagrams show the best match of all observables analyzed simultaneously in our study. In the thermodynamic limit of infinitely long chains the transitions are expected to occur at sharp values of the parameters. For finite chains, on the other hand, the transition lines still vary with chain length  $N$  and are not well defined because of broad peaks in the observables that also have small differences in between. Therefore the locations of the phase boundaries should be considered as a rough guide. However, even for the rather short chains considered here, we can clearly identify different phases which show distinguishing features, so that a reasonable picture is obtained. Most of the phases are believed to still persist for longer chains. All our results obtained from the different observables are summarized in the phase diagrams in the  $R_s - T$  plane which for a convenient overview are displayed at the beginning of the results section in Fig. 3(a) for non-grafted and in Fig. 3(b) for end-grafted polymers, respectively.

It is clear that, for longer chains, the desorbed, globule and compact phases will survive. Additionally, filmlike (monolayer) and semispherical conformations (two layer), as well as surface attached globular shapes will dominate the respective phases. On the other hand, as long as surface effects are as influential as volume effects the compact adsorbed conformations differ noticeably for polymers with different but small lengths. But, for the majority of phases we find qualitative coincidence with a simple coarse-grained model.

In this study, we kept the adsorption field constant (whereas we varied the adsorption strength in another earlier study) and varied the radius of the nano-particles and observed qualitatively the described scenarios. As a result, our model system can be mapped in the considered parameter range to real systems considered in experiments.

For example, based on early experimental results [85, 86], Feng and Ruckenstein [43] examined the adsorption of a specific polyampholyte chain on a single spherical nano-particle with three different radii. In this application, the charge density at the particle surface regulates the strength of the adsorption field (corresponding to our parameter  $\epsilon$ ) and the polymer composition regulates the location of the coil-globule transition (corresponding to  $\epsilon_{LJ}$ ). Compared with experimental findings, computational studies of generic coarse-grained models have the advantage that different combinations of parameters can be varied over wide ranges. In this way, a specific detailed system can be put into a broader context and a deeper understanding based on fundamental principles of statistical physics can be gained.

## ACKNOWLEDGMENTS

We wish to thank Viktoria Blavatska and Bernd Abel for useful discussions. H.A. acknowledges support by the Alexander von Humboldt Foundation under the Experienced Researcher Fellowship Programme. W.J. thanks the German Research Foundation (DFG) for support under Grant Nos. JA483/24-3 and SFB/TRR 102 (Project B04). We also benefitted from the Marie Curie IRSES network DIONICOS under Contract No. PIRSES-GA-2013-612707 within the European Union Seventh Framework Programme. The computer time for the Monte Carlo simulations was provided by NIC, Forschungszentrum Jülich, under Grant No. hlz24, which we gratefully acknowledge.

- 
- [1] R. F. Service, *Science* **270**, 230 (1995).
  - [2] S. Walheim, E. Schaffer, J. Mlynek, and U. Steiner, *Science* **283**, 520 (1999).
  - [3] S. Brown, *Nature Biotechnol.* **15**, 269 (1997).
  - [4] R. Braun, M. Sarikaya, and K. Schulten, *J. Biomater. Sci. Polymer Edn.* **13**, 747 (2002).
  - [5] S. R. Whaley, D. S. English, E. L. Hu, P. F. Barbara, and A. M. Belcher, *Nature* **405**, 665 (2000).
  - [6] K. Goede, P. Busch, and M. Grundmann, *Nano Lett.* **4**, 2115 (2004).
  - [7] M. Bachmann, K. Goede, A. G. Beck-Sickingler, M. Grundmann, A. Irbäck, and W. Janke, *Angew. Chem. Int. Ed.* **49**, 9530 (2010).
  - [8] E. Eisenriegler, K. Kremer, and K. Binder, *J. Chem. Phys.* **77**, 6296 (1982).
  - [9] R. Descas, J.-U. Sommer, and A. Blumen, *J. Chem. Phys.* **120**, 8831 (2004).
  - [10] M. Bachmann and W. Janke, *Phys. Rev. Lett.* **95**, 058102 (2005).
  - [11] M. Bachmann and W. Janke, *Phys. Rev. E* **73**, 020901(R) (2006).
  - [12] M. Bachmann and W. Janke, *Phys. Rev. E* **73**, 041802 (2006).
  - [13] J. Luettmer-Strathmann, F. Rampf, W. Paul, and K. Binder, *J. Chem. Phys.* **128**, 064903 (2008).
  - [14] M. Bachmann and W. Janke, in: *Rugged Free Energy Landscapes: Common Computational Approaches to Spin Glasses, Structural Glasses and Biological Macromolecules*, edited by W. Janke, *Lect. Notes Phys.* **736** (Springer, Berlin, 2008); pp. 203–246.
  - [15] M. Möddel, M. Bachmann, and W. Janke, *J. Phys. Chem. B* **113**, 3314 (2009).
  - [16] V. A. Ivanov, J. A. Martemyanova, M. Müller, W. Paul, and K. Binder, *J. Phys. Chem. B* **113**, 3653 (2009).
  - [17] T. Chen, L. Wang, X. Lin, Y. Liu, and H. Liang, *J. Chem. Phys.* **130**, 244905 (2009).
  - [18] L. Wang, T. Chen, X. Lin, Y. Liu, and H. Liang, *J. Chem. Phys.* **131**, 244902 (2009).
  - [19] A. D. Swetnam and M. P. Allen, *Phys. Chem. Chem. Phys.* **11**, 2046 (2009).
  - [20] M. Möddel, W. Janke, and M. Bachmann, *Phys. Chem. Chem. Phys.* **12**, 11548 (2010).
  - [21] M. Möddel, W. Janke, and M. Bachmann, *Macromolecules* **44**, 9013 (2011).
  - [22] V. Blavatska and W. Janke, *J. Chem. Phys.* **136**, 104907 (2012).
  - [23] Y. W. Li, T. Wüst, and D. P. Landau, *Phys. Rev. E* **87**, 012706 (2013).
  - [24] M. Möddel, W. Janke, and M. Bachmann, *Phys. Rev. Lett.* **112**, 148303 (2014).
  - [25] M. P. Taylor and J. Luettmer-Strathmann, *J. Chem. Phys.* **141**, 204906 (2014).
  - [26] K. S. Austin, J. Zierenberg, and W. Janke, *Macromolecules* **50**, 4054 (2017).
  - [27] J. Krawczyk, A. L. Owczarek, T. Prellberg, and A. Reznitz, *J. Stat. Mech.: Theory Exp.*, P05008 (2005).
  - [28] S. Bhattacharya, V. G. Rostiashvili, A. Milchev, and T. A. Vilgis, *Phys. Rev. E* **79**, 030802(R) (2009).
  - [29] M. J. Russell, *Science* **302**, 580 (2003).
  - [30] M. Lundqvist, P. Nygren, B.-H. Jonsson, and K. Broo, *Angew. Chem. Int. Ed.* **45**, 8169 (2006).
  - [31] I. Gurevitch and S. Srebnik, *Chem. Phys. Lett.* **444**, 96 (2007).
  - [32] I. Gurevitch and S. Srebnik, *J. Chem. Phys.* **128**, 144901 (2008).
  - [33] T. Vogel and M. Bachmann, *Phys. Rev. Lett.* **104**, 198302 (2010).
  - [34] T. Vogel, J. Gross, and M. Bachmann, *J. Chem. Phys.* **142**, 104901 (2015).
  - [35] M. Tagliazucchi, M. Olvera de la Cruz, and I. Szleifer, *Proc. Natl. Acad. Sci. U.S.A.* **107**, 5300 (2010).
  - [36] R. R. Netz and J.-F. Joanny, *Macromolecules* **31**, 5123 (1998).
  - [37] S. A. Barr and A. Z. Panagiotopoulos, *J. Chem. Phys.* **137**, 144704 (2012).
  - [38] A. Gladytz, M. Wagner, T. Häupl, C. Elsner, and B. Abel, *Part. Part. Syst. Char.* **32**, 573 (2015).

- [39] C. Elsner, D. Hintzen, A. Prager, K. R. Siefertmann, and B. Abel, *Z. Phys. Chem.* **229**, 427 (2015).
- [40] A. Gladytz, B. Abel, and H. J. Risselada, *Angew. Chem. Int. Ed.* **55**, 11242 (2016).
- [41] M. Tanaka, A. Yu. Grosberg, and T. Tanaka, *J. Chem. Phys.* **110**, 8176 (1999).
- [42] M. Tanaka and T. Tanaka, *Phys. Rev. E* **62**, 3803 (2000).
- [43] J. Feng and E. Ruckenstein, *Polymer* **44**, 3141 (2003).
- [44] J. McNamara, C. Y. Kong, and M. Muthukumar, *J. Chem. Phys.* **117**, 5354 (2002).
- [45] J. Wang and M. Muthukumar, *J. Chem. Phys.* **135**, 194901 (2011).
- [46] R. Messina, *Macromolecules* **37**, 621 (2004).
- [47] A. V. Dobrynin and M. Rubinstein, *Prog. Polym. Sci.* **30**, 1049 (2005).
- [48] A. V. Dobrynin, *Curr. Opin. in Colloid and Interface Sci.* **13**, 376 (2008).
- [49] R. R. Netz and J.-F. Joanny, *Macromolecules* **32**, 9013 (1999).
- [50] R. R. Netz and D. Andelman, *Phys. Rep.* **380**, 1 (2003).
- [51] M. Marenz, J. Zierenberg, H. Arkin, and W. Janke, *Condens. Matter Phys.* **15**, 43008 (2012).
- [52] H. Arkin and W. Janke, *Phys. Rev. E* **85**, 051802 (2012).
- [53] H. Arkin and W. Janke, *J. Chem. Phys.* **138**, 054904 (2013).
- [54] H. Arkin and W. Janke, *J. Phys. Chem. B* **116**, 10379 (2012).
- [55] H. Arkin and W. Janke, *Eur. Phys. J. – Special Topics* **216**, 181 (2013).
- [56] T. Bogner, A. Degenhard, and F. Schmid, *Phys. Rev. Lett.* **93**, 268108 (2004).
- [57] E. Balog, T. Becker, M. Oettl, R. Lechner, R. Daniel, J. Finney, and J. C. Smith, *Phys. Rev. Lett.* **93**, 028103 (2004).
- [58] M. Ikeguchi, J. Ueno, M. Sato, and A. Kidera, *Phys. Rev. Lett.* **94**, 078102 (2005).
- [59] N. Gupta and A. Irbäck, *J. Chem. Phys.* **120**, 3983 (2004).
- [60] F. H. Stillinger, T. Head-Gordon, and C. L. Hirshfeld, *Phys. Rev. E* **48**, 1469 (1993).
- [61] F. H. Stillinger and T. Head-Gordon, *Phys. Rev. E* **52**, 2872 (1995).
- [62] A. Irbäck, C. Peterson, F. Potthast, and O. Sommelius, *J. Chem. Phys.* **107**, 273 (1997).
- [63] A. Irbäck, C. Peterson, and F. Potthast, *Phys. Rev. E* **55**, 860 (1997).
- [64] M. Bachmann, H. Arkin, and W. Janke, *Phys. Rev. E* **71**, 031906 (2005).
- [65] M. Marenz and W. Janke, *Phys. Rev. Lett.* **116**, 128301 (2016).
- [66] S. J. Marrink, H. J. Risselada, S. Yefimov, D. P. Tieleman, and A. H. de Vries, *J. Phys. Chem. B* **111**, 7812 (2007).
- [67] A. L. Rodriguez, C. Vega, and J. J. Freire, *J. Chem. Phys.* **111**, 438 (1999).
- [68] B. A. Berg and T. Neuhaus, *Phys. Lett. B* **267**, 249 (1991).
- [69] B. A. Berg and T. Neuhaus, *Phys. Rev. Lett.* **68**, 9 (1992).
- [70] W. Janke, *Int. J. Mod. Phys. C* **3**, 1137 (1992).
- [71] B. A. Berg, *Fields Inst. Commun.* **28**, 1 (2000).
- [72] W. Janke, *Physica A* **254**, 164 (1998).
- [73] W. Janke, in: *Computer Simulations of Surfaces and Interfaces*, NATO Science Series, II. Mathematics, Physics and Chemistry – Vol. **114**, edited by B. Dünweg, D. P. Landau, and A. I. Milchev (Kluwer, Dordrecht, 2003), pp. 137–157.
- [74] W. Janke and W. Paul, *Soft Matter* **12**, 642 (2016).
- [75] J. Zierenberg, M. Marenz, and W. Janke, *Polymers* **8**, 333 (2016).
- [76] K. Solc and W. H. Stockmayer, *J. Chem. Phys.* **54**, 2756 (1971).
- [77] D. N. Theodorou and U. W. Suter, *Macromolecules* **18**, 1206 (1985).
- [78] V. Blavatska and W. Janke, *J. Chem. Phys.* **133**, 184903 (2010).
- [79] J. Vymětal and J. Vondrášek, *J. Phys. Chem. A* **115**, 11455 (2011).
- [80] V. Blavatska and W. Janke, *J. Chem. Phys.* **136**, 104907 (2012).
- [81] B. Efron, *The Jackknife, the Bootstrap and Other Resampling Plans* (Society for Industrial and Applied Mathematics [SIAM], Philadelphia, 1982).
- [82] W. Janke, *Monte Carlo methods in classical statistical physics*, in: *Computational Many-Particle Physics*, Wilhelm & Else Heraeus Summerschool, Greifswald, edited by H. Fehske, R. Schneider, and A. Weiße, *Lect. Notes Phys.* **739** (Springer, Berlin, 2008), pp. 79–140.
- [83] W. Janke, *Monte Carlo simulations in statistical physics – From basic principles to advanced applications*, in: *Order, Disorder and Criticality: Advanced Problems of Phase Transition Theory*, Vol. 3, edited by Y. Holovatch (World Scientific, Singapore, 2012), pp. 93–166.
- [84] E. Eisenriegler, K. Kremer, and K. Binder, *J. Chem. Phys.* **77**, 6296 (1982).
- [85] V. Lesins and E. Ruckenstein, *Colloid Polym. Sci.* **266**, 1187 (1988).
- [86] V. Lesins and E. Ruckenstein, *J. Colloid Interface Sci.* **132**, 566 (1989).

# Supplementary Material for: Polymer Adsorption on Curved Surfaces

Handan Arkin<sup>1,2,\*</sup> and Wolfhard Janke<sup>1,†</sup>

<sup>1</sup>*Institut für Theoretische Physik, Universität Leipzig, Postfach 100 920, D-04009 Leipzig, Germany*

<sup>2</sup>*Department of Physics Engineering, Faculty of Engineering, Ankara University, Tandogan, 06100 Ankara, Turkey*

Next to the expectation values  $\langle O \rangle$  of all structural quantities in our main text, we also determined the fluctuations of these structural quantities, as represented by the temperature derivative  $d\langle O \rangle/dT = (\langle OE \rangle - \langle O \rangle \langle E \rangle) / T^2$ . We use generic units, in which  $k_B = 1$ . The fluctuations of all structural quantities not discussed in the main text are given in the following figures:

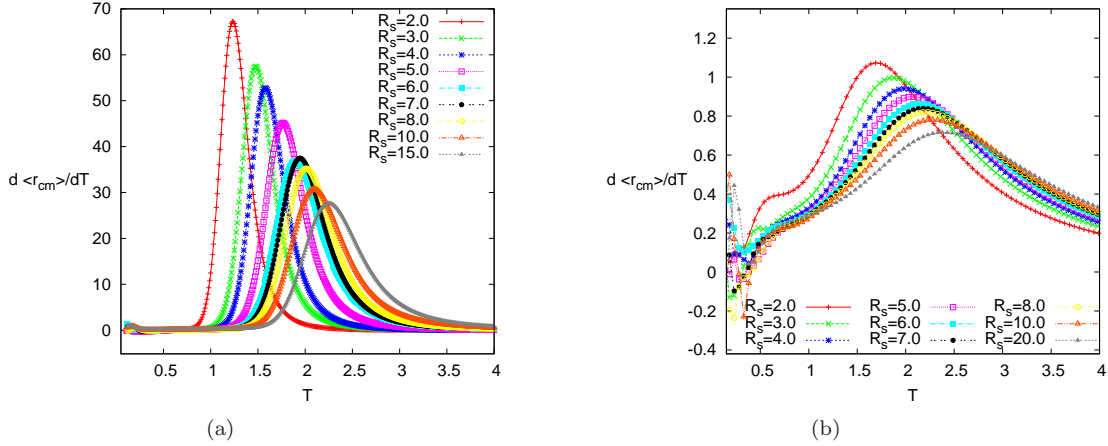


FIG. 1: (Color online) The fluctuations of the distance of the center-of-mass of the polymer from the sphere surface for (a) the non-grafted and (b) the end-grafted case.

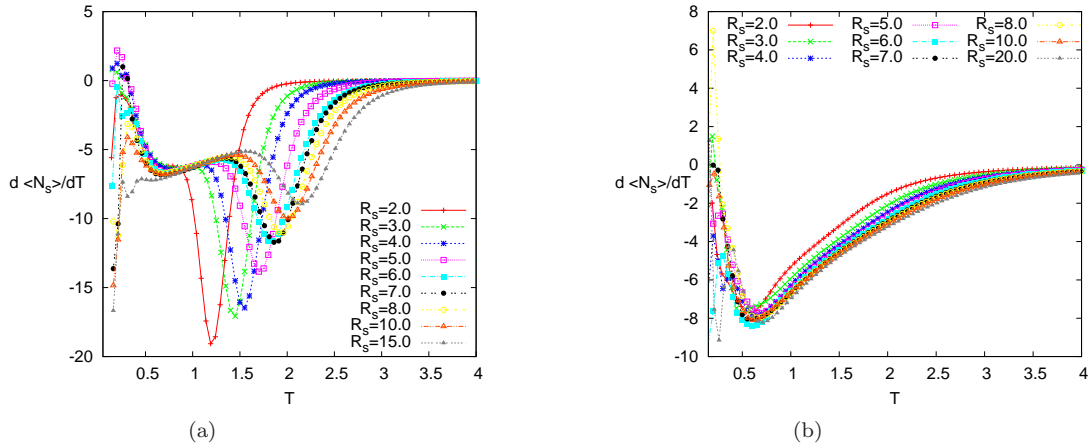


FIG. 2: (Color online) The fluctuations of the number of adsorbed monomers for (a) the non-grafted and (b) the end-grafted case.

\*E-mail: Handan.Olgar@eng.ankara.edu.tr

†E-mail: Wolfhard.Janke@itp.uni-leipzig.de;

Homepage: <http://www.physik.uni-leipzig.de/CQT.html>

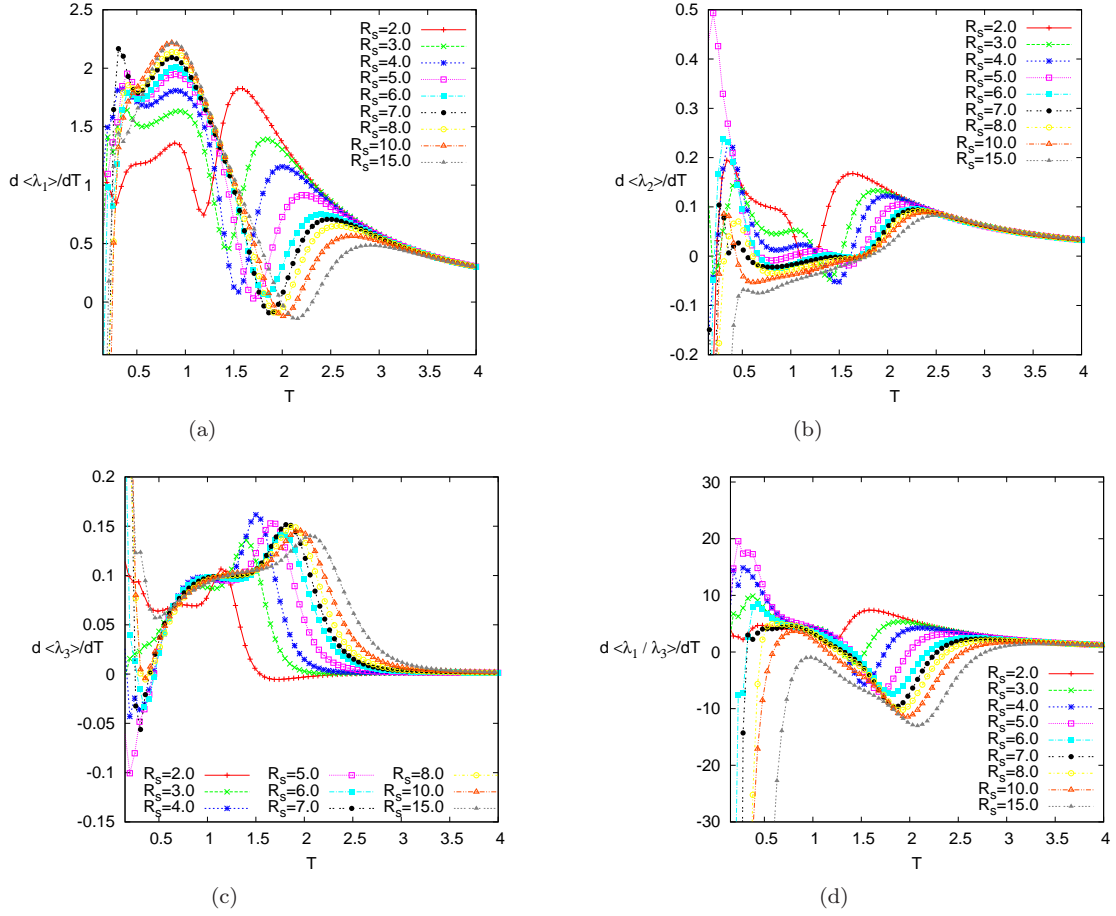


FIG. 3: (Color online) The fluctuations of the three eigenvalues (a)  $\langle\lambda_1\rangle$ , (b)  $\langle\lambda_2\rangle$ , (c)  $\langle\lambda_3\rangle$  of the gyration tensor and (d) the fluctuations of the ratio of the largest eigenvalue to the smallest eigenvalue  $\langle\lambda_1/\lambda_3\rangle$  for different sphere radii  $R_s$  for the non-grafted case.